Planetary Cratering Mechanics

*John D. O'Keefe and Thomas J. Ahrens**

Lindhurst Laboratory of Experimental Geophysics
Seismological Laboratory, California Institute of Technology
Pasadena, CA 91125

*Correspondent

ABSTRACT

To obtain a quantative understanding of the cratering process over a broad range of conditions, we have numerically computed the evolution of impact induced flow fields and calculated the time histories of the major measures of crater geometry (e.g. depth diameter, lip height. . .) for variations in planetary gravity (0 to 10^9cm/s^2), material strength (0 to 140 kbar), thermodynamic properties, and impactor radius (0.05 to 5000 km). These results were fit into the framework of the scaling relations of Holsapple and Schmidt [1987].

We describe the impact process in terms of four regimes: (1) penetration, (2) inertial, (3) terminal and (4) relaxation. During the penetration regime, the depth of impactor penetration grows linearly for dimensionless times $\tau = (Ut/a) < 5.1$. Here, U is projectile velocity, t is time, and "a" is projectile radius. In the inertial regime, $\tau > 5.1$, the crater grows at a slower rate until it is arrested either by strength or gravitational forces. The crater depth, D, and diameter, d, normalized by projectile radius is given by $D/a = 1.3\ (Ut/a)^{0.36}$ and $d/a = 2.0 = (Ut/a)^{0.36}$. For strength dominated craters, growth stops at the end of the inertial regime, which occurs at $(Y_{eff}/\rho U^2)^{-0.78}$, where Y_{eff} is the effective planetary crustal strength. In gravity dominated craters, growth stops when the gravitational forces dominate over the inertial, which occurs at $\tau = 0.92\ (ga/U^2)^{-0.61}$. In strength dominated craters, the growth stops at the end of the inertial regime, which occurs at $\tau = 0.33\ (Y_{eff}/\rho U^2)^{-0.78}$. In the gravity and strength regimes the maximum depth of penetration is $D_p/a = 1.2\ (ga/U^2)^{-0.22}$ and $D_p/a = 0.84\ (Y/\rho\ U^2)^{-0.28}$, respectively.

The transition form simple bowl-shaped craters to complex-shaped crater is found to result from the transition from strength dominated to gravity dominated craters. The diameter for this transition to occur is given by $d_T = Y/\rho g$, and thus scales as g^{-1} for planetary surfaces where strength is not strain-rate dependent. This result agrees with crater-shape data for the terrestrial planets [Chapman and McKinnon, 1986].

We have related some of the calculable, but non-observable parameters which characterize the cratering process (e.g. maximum depth of penetration, depth of excavation, and maximum crater lip height) to the crater diameter. For example, the maximum depth of penetration relative to the maximum crater diameter is 0.58, for strength dominated craters, and 0.28 for gravity dominated craters. These values imply that impactors associated with the large basin impacts penetrated relatively deeply into the planet's surface. This significantly contrasts to earlier hypotheses in which it had been erroneously inferred from structural data that the relative transient crater penetration decreased with increasing diameter. Similarly, the ratio of the maximum depth of excavation relative to the crater diameter is a constant $\equiv 0.1$, for gravity dominated craters, and $\equiv 0.2$ for strength dominated craters. This result implies that for threshold impact velocities less than 25 km/sec, where significant vaporization begins to take place, the excavated material comes from a maximum depth of 0.1 times the transient crater diameter Moreover, we find apparent final crater diameter is approximately twice the transient crater diameter at diameters of greater than $d_t = 8.6\ Y/\rho g$.

INTRODUCTION

The recent decades of planetary observation and exploration have lead to the conclusion that the impact of solid bodies is one of the fundamental processes in the origin and evolution of the solar system.While the impact process is conceptually easy to visualize, the detailed quantitative description of the mechanics has been difficult and illusive (e.g. Melosh [1989]). The overall objective of this study is to obtain a quantative understanding of the planetary cratering process over a broad range of conditions. Specifically the objectives are to establish quantitative scaling relationships for: (1) the temporal evolution of the key measures of the crater geometry (depth, diameter, and lip height), (2) the maximum depth of penetration and excavation, and (3) the transition from simple to complex craters. We address these objectives over a broad range of planetary gravities, material strengths, and impactor sizes (from meters to those that formed the multiringed basins).

APPROACH AND SCOPE

We modeled the normal impact of spherical projectiles on a semi-infinite planet surface over a broad range of conditions using numerical techniques. We do not address the effect of a planet's atmosphere upon the cratering process in the present paper and refer readers to [Melosh, 1989 Chapt. XI; O'Keefe and Ahrens, 1988; Roddy et al., 1987; Schultz and Gault, 1981]. To calculate the impact-induced flow fields within the solid planets, we used the Eulerian-Lagrangian code developed by Thompson [1979]. The key equation of state parameters along with the mechanical parameters that were used in the code to represent a typical silicate impactor and planet are listed in Table 1. The constitutive model accounted for elastic-plastic hydrodynamic responses [Thompson, 1979]. Other models are being examined and will be reported upon in the future. We varied some of the equation of state parameters such as the melt enthalpy and vaporization enthalpy, and also

the mechanical properties such as the yield strength. In all cases, the material properties of the impactor and planet were identical.

The impact parameters and variables are listed in Table 1 along with the range over which they were varied. We nondimensionalized these using the formalism of Holsapple and Schmidt [1987]. The magnitudes of the four dimensionless parameters ga/U^2, $Y/\rho U^2$, H_m/U^2 and H_{vap}/U^2 are measures of the dominant mechanisms controlling the cratering process. We varied these parameters over a range of conditions so as to determine when each of these was the dominant parameter that described the impact process.

The inverse Froúde number, ga/U^2, is a measure of the gravitational forces relative to the pressure forces. The inverse Cauchy number, $Y/\rho U^2$, is a measure of the planetary strength relative to the pressure forces; and the melt, H_m/U^2, and vaporization, H_{vap}/U^2, numbers are measures of the relative importance of melting and vaporization. In determining the range of the inverse Froúde number, we had a choice of varying either the projectile radius or the gravitational acceleration; for ease of computation, we fixed the radius and varied the gravitational acceleration over six orders of magnitude. This is equivalent to varying the impactor radius from 5 m to 5000 km. In determining the range of the vaporization number, H_{vap}/U^2, we restricted the impact velocities to 12 km/s so as to not get into the impact regime where there are significant vaporization effects. This limits the validity of the scaling laws to velocities less than 30 km/s for typical silicates. We have studied the effects of high speed impacts (>30 km/s) and will report in detail on these elsewhere [O'Keefe and Ahrens, 1989].

The results of the computations represent a very large amount of computer output with over $\sim 10^4$ variables being calculated for each time step. In this paper we will report on the geometrical measures of the cratering process such as the depth, diameter and lip height. The depth is defined as the distance from the initial planetary surface and the planetary surface at a given time at the centerline of the impact; the diameter is defined as

the distance between the interface between the impactor and planetary surface at the initial planetary surface height; the lip height is measured relative to the original planetary surface level (e. g. see figure 1). The dimensionless depth and diameter histories are summarized in Table 2. In addition, we have included a series of detailed flow field plots; these represent the development of a simple bowl shaped crater (figure 1) and a complex crater exhibiting central peak and ring formation (figure 2) .To determine the displacement of planetary material during the cratering process, we placed massless tracer particles at various positions and computed their trajectories which are also shown.

CRATER SCALING REGIMES

The cratering process can be described in terms of at least four temporal regimes; penetration, inertial, terminal and relaxation. Schmidt and Holsapple called these first three regimes the early stage, intermediate and late. The numerical approach taken here can be used to describe the first three; the fourth, the terminal regime is the result of long term equilibration and requires a different analytical approach such as viscous relaxation methods (e.g. Melosh [1989], Chapt. 8). In the following section we will describe the first three regimes and determine the numerical values of the parameters in the Holsapple and Schmidt [1987] scaling laws. We will describe the depth, diameter, and other geometrical measures in that order. The scaling laws and the numerical values of the parameters derived from the present calculations are listed in Table 3.

PENETRATION REGIME

The penetration regime is characterized by the transfer of the kinetic energy of the projectile to the planetary surface. In the case where the impactor and planetary surface have similar properties, about half of the impactor kinetic energy is transferred to the planet during the penetration regime [O'Keefe and Ahrens, 1977]. During this time, the impactor drives a strong shock wave into the planet and also deforms and lines the growing crater

cavity wall (Figures 1a,b). The material properties of the impactor and the planet and the planet's gravitational acceleration are not important during this time, except for relative differences in density between the impactor and the planet [Holsapple and Schmidt, 1987].

Depth

The crater depth grows linearly with time in the penetration regime. Shown in Figure 3 is a plot of the evolution of the interface between the impactor and the planet at the centerline of impact for a wide range of impact conditions. Note that all the cases fall on a single line independent of strength or gravitational acceleration. This linear growth is expected during the early times when the shock at the interface is nearly planar and is predicted from planar shock wave theory. The depth(D)/impactor radius(a) evolves as

$$D/a = \frac{1}{2}(Ut/a) \qquad (1)$$

where U is the impact velocity. The factor of two comes from the fact that upon impact of bodies of like impedances, the interface velocity is one-half the impactor velocity.

The depth grows linearly with time until it enters the inertial regime This was predicted by Holsapple and Schmidt [1987] to occur at dimensionless time, τ, of 5.1 for like impacts and this is substantiated in Figure 3.

Diameter

The diameter does not have a simple growth law during the penetration regime. The impact of a near spherical impactor will produce small amounts of jetting and vaporization near the initial point of impact even at low velocities; the magnitude depends sensitively on the details of the impactor-planetary surface geometry [Kieffer, 1976]. The penetration regime for diameter ends when the maximum lateral extent of the impactor penetrates the surface which, from geometrical considerations for a spherical impactor, occurs at dimensionless time of

$$\tau = Ut/a = 2 \qquad (2)$$

Shape

The shape of the transient cavity changes rapidly during the penetration regime. The depth grows more rapidly than the diameter during the penetration time for the depth, and the scaling of the evolution of the diameter to depth is given from the ratio of equations 1 and 6

$$d/D = 4.0\ (\ Ut/a\ )^{-0.64} \quad ; \quad 1 < (\ Ut/a\ ) < 5.1 \qquad (3)$$

INERTIAL REGIME

The inertial regime is characterized by the quasi-hemispherical expansion of the crater cavity. In this regime, the geometry of the cavity does not change, and the projectile is deformed into a thin hemispherical shell that lines the transient crater cavity. The strong shock that was attached to the projectile during the penetration time has now propagated away from the the cavity region [Bjork, 1961; O'Keefe and Ahrens, 1977]. Bjork called this regime the detached shock regime. As in the penetration regime, the material strength properties and gravity do not play a role in the evolution, however, the termination of this regime occurs when either strength or gravitational effects arrest crater growth.

Depth

The depth grows as a simple power law in the inertial regime and it is independent of either strength or gravitational acceleration (see Figure 3). A similar result for the depth was found by Holsapple and Schmidt [1987 Figure 4] for a variety of impact conditions. Eq. 4 is obtained by fitting the depth versus time curve (Fig. 3) in the inertial regime. The scaling law is given by

$$D/a = 1.3\ (Ut/a)^{0.36} \qquad (4)$$

The magnitude of the inertial regime exponent (s=0.36) is related to the coupling coefficient of Holsapple and Schmidt [1987] by the relation

$$\mu = s/(1-s) \qquad (5)$$

Eq. 5 gives $\mu = 0.56$, which is consistent with the range of values found by Holsapple and Schmidt [1987] for a range of impact conditions. In the following sections all of the scaling laws will have exponents that are functions of μ and thus are related to the exponent in the inertial regime.

Diameter

The diameter also grows as a simple power law in the inertial regime (e.g. Figure 4). The scaling for the diameter from a fit to the results in Fig. 4 is given by

$$d/a = 2.0\ (Ut/a)^{0.36} \qquad (6)$$

Note that the exponent is the same for both the depth and diameter.

Shape

The shape is similar throughout the duration of the inertial regime. The ratio of the diameter to depth is

$$d/D = 1.6 \quad : \quad 1<(Ut/a)< t_{mp} \qquad (7)$$

where t_{mp} is the time of maximum penetration. This time is specified in Eq. 8 below.

TERMINAL REGIME

The growth in inertial regime is arrested by strength and gravitational forces, and this marks the beginning of the terminal regime. In the case of simple craters (Figure 1), the final shape of the crater is reached at the end of the inertial regime with the exception of the collapsing and folding over of the crater lip and minor elastic rebounding. In the case of complex craters (Figure 2), the end of the inertial regime marks the beginning of a series of complex motions which subsequently occur. These motions include the rebounding of the crater floor and the formation of central peaks and the collapse and propagation of the crater lip to form ringed craters.

Depth

The beginning of the terminal regime for crater depth occurs at the time of maximum penetration, t_{mp}. This time, in the case where the gravitational forces dominant over the strength forces, is given by

$$Ut_{mp}/a = 0.92 \, (ga/U^2)^{-0.61} \qquad (8)$$

where the exponent magnitude is given by $(1+\mu)/(2+\mu)$. The proportionality constant is obtained by fitting the results shown in Fig. 3.

The maximum in the depth of penetration in the gravity dominated case is a function of the inverse Froúde number and is obtained from Figure 5. The associated scaling law is given by

$$D_p/a = 1.2 \, (ga/U^2)^{-0.22} \qquad (9)$$

where the exponent is given by $\mu/(2+\mu)$ and the proportionality contant is obtained from the results shown in Figure 5.

The beginning of the terminal regime or the time of maximum penetration t_{mp}, in the case where strength forces are dominant is given by

$$Ut_{mp}/a = 0.33 \, (Y_{eff}/\rho U^2)^{-0.78} \qquad (10)$$

where the exponent is $(1+\mu)/2$ Here Y_{eff} is equal to twice the maximum shear strength. For the crusts of typical cratered planetary surfaces, we expect Y_{eff} will be significantly diminished from data from tests on undamaged rock on account of shock-induced cracking (e.g. Simmons et al. [1973] and Ahrens and Rubin [1992]). The temporal evolution in the strength dominated regime is shown in Fig. 6 from which Eq. 10 is derived by fitting the peaks of D/a versus Ut/a relations shown in Fig. 6.

The maximum depth of penetration in the strength dominated case is a function of the inverse Cauchy number and is shown in Figure 7. The depth follows a power law with an expected slope given by $\mu/2 = 0.28$ until the inverse Cauchy number approaches ~ 10^{-2}. This change in scaling is a result of increased importance of shock weakening of the planetary material in the cratering process. Weakening is a result of the irreversible work

done in by the shock and subsequent unloading process and as a result of the post-shock deformation of the rock surrounding the crater. The irreversible work will result from both thermal shock heating and mechanical fracturing effects and is more intense close to the impact point where the high shock stresses are experienced. The importance of shock weakening depends upon the planetary strength, thermal state, and impact velocity. In the case of weak planetary crusts, and low impact velocities, the volume of the final crater is much greater than the shock weakened region and the effect is minor. However in the case of very strong initial crustal strengths, high surface temperatures or high (>30 km/sec) impact velocities, the extent of the shock weakening is comparable to the crater size, and the shock weakening effect can dominate late crater growth and the entire size and shape of the final crater.

Shock weakening was modeled as thermal weakening and did not account for fracturing, which is currently an area of active interest (e.g.[Ahrens and Rubin, 1992; Asphaug et al., 1991; Housen and Holsapple, 1990]) and the present work should be extended to include that effect. Our code computed the temperature field at each time step. The local temperature was used to compute the degree of thermal weakening by reducing the local strength in proportion to the difference between temperature and the melt temperature where the strength vanishes. The results of the code runs are plotted in Fig. 7 for both depth of penetration and diameter.

In the strength dominated case where shock weakening is negligible, the scaling is given by

$$D_p/a = 0.84 \left(Y/\rho U^2 \right)^{-0.28} \qquad (11)$$

which is derived from Fig. 7.

In the shock weakened case, the depth is independent of the magnitude of the yield strength and is determined by the amount of material that is thermally weakened. In this case, the depth of penetration scaling is similar to depth of melting scaling [Bjorkman, 1983] and is given by

$$D_p/a = 0.70 \, (H_m/U^2)^{-0.28} \quad (12)$$

where H_m is the enthalpy required to induce shock melting, which in the case of thermal weakening is equal to the enthalpy to melt as referenced to the planets' ambient surface condition. The constants in Eq. 12 are obtained from fitting the calculational results of Fig. 8. The exponent is $\mu/2$, which is identical to the strength case.

The condition for the transition between the strength and the shock weakened regimes can be obtained by equating Eqs. 11 and 12, which gives

$$Y/\rho H_m = 0.25 \quad (13)$$

A general relationship for depth that accounts for both regimes can be obtained by adding Eqs. 11 and 12 which yields

$$D_p/a = K_s \, (Y/\rho U^2)^{-0.28} + K_{sw} \, (H_m/U^2)^{-0.28} \quad (14)$$

where $K_s = 0.84$ and $K_{sw} = 0.7$. This relationship can be plotted over a range of values relevant to planetary surfaces and is shown in Fig. 8. Eq. 14 implies an effective strength which accounts for shock weakening which can be defined as

$$Y_{eff} = Y \, \{ \, 1 + (K_{sw}/K_s) \, (Y/\rho H_m)^{0.28} \}^{(-1/0.28)} \quad (15)$$

This result is plotted in Figure 9.

A general interpolation relationship of the form suggested by Holsapple and Schmidt [1987] can be used to span the gravity and strength regimes

$$D_p/a = K_s \, (ga/U^2)^{-0.22} \, \{ \, (K_g/K_s)^{-0.22} + (Y/\rho U^2)^{(0.22/0.28)} \, (ga/U^2)^{-1} \, \}^{-0.22} \quad (16)$$

where $K_g = 1.2$.

Replacing the shear strength by the effective strength defined in Eq. 15 leads to a more general scaling relationship that includes gravity, strength and shock weakening effects

$$D_p/a = K_s \, (ga/U^2)^{-0.22} \{ (K_g/K_s)^{-0.22} + \{ \, (Y/\rho U^2) \, \{ \, 1 + (K_{sw}/K_s) \, (Y/\rho H_m)^{0.28} \, \}^{-1/0.28)} \, (0.22/0.28) \, (ga/U^2)^{-1} \}^{-0.22} \} \quad (17)$$

The maximum depth of penetration of projectiles from giant impacts has been a topic of much debate in the literature (e.g. Grieve et al.[1981]). The tracer particles

employed in the calculations help elucidate the motions of material in the cratering process. Referring to Figs. 1 and 2, we see that near the centerline of impact, planetary material is driven downward and is not ejected in the cratering process. As one moves from the centerline towards the crater lip, there is a region in which the planetary material is essentially stagnated against the outwardly moving cavity wall; this stagnated region, delineated by layers of tracer particles, shows a lower layer of particles being driven downward and an upper layer moving upward and being excavated (see Fig. 1c). The scaling laws for the maximum depth of excavation is given by

$$D_{ex}/a = 0.17\ (Y/\rho U^2)^{-0.28} \qquad (18a)$$

and

$$D_{ex/a}=K(ga/U2)^{-0.22} \qquad (18b)$$

for the strength dominated regime. Here the exponents for strength and gravity scaling are given by Eqs. 11 and 12. The proportional constant is obtained from Figs. 2 and 3.

Diameter

The beginning of the terminal regime for the diameter occurs when the crater lip stops expanding laterally. In the case where the gravitational forces are dominant, this occurs when

$$Ut/a = 1.8\ (\ ga/U^2)^{-0.61} \qquad (19)$$

where the exponent magnitude is given by $(1+\mu)/(2+\mu)$ and the proportionality factor in this equation and those of Eqs. 20 and 21, below, come from fitting the results of Fig. 4.

An example of the crater morphology at the time the crater cavity has reached its maximum diameter in the gravity dominated case is shown in Figure 2c. The cavity maximum diameter is a function of the inverse Froúde number and is given by

$$d_m/a = \ 2.1\ (\ ga/U^2)^{-0.22} \qquad (20)$$

where the exponent is $\mu/(2+\mu)$.

At the time the crater cavity has reached its maximum diameter, the crater lip has reached its maximum height (figure 2c). This height scales as

$$H_\ell/a = \quad 0.53\ (\ ga/U^2)^{-0.22} \tag{21}$$

where the exponent is again $\mu/(2+\mu)$where the proportionality factor was obtained from plots such as Fig. 2c.

The crater lip will collapse and produce an outwardly propagating surface wave which rapidly increases the apparent diameter of the crater (Figs. 2c-2d). Simultaneously, the crater floor moves upward and an inner crater lip forms. Note that neither the outer ring nor the inner ring correspond to the maximum diameter of the transient crater.

The diameter of the outer ring scales as

$$d/a = 4.28\ (\ ga/U^2)^{-0.22} \tag{22}$$

where as before the exponent is given by $\mu/(2+\mu)$. The proportionality factor comes from Eq. 4.

When strength dominates the cratering process, the crater growth ends in the inertial regime with only a small amount of elastic rebounding occurring followed by long term crater relaxation. The time of termination of crater formation is given by

$$Ut/a = 0.33\ (\ Y_{eff}/\rho U^2)^{-0.78} \tag{23}$$

Note that this time is identical to that for the depth. The parameters come from fitting the results of Fig. 6.

The maximum or final crater diameter in the strength dominated regime is given by

$$d/a = 1.4\ \ (\ Y/\rho U^2)^{-0.28} \tag{24}$$

Here we employed the results shown in Fig. 7. In the shock weakened regime the final diameter is given by

$$d/a = \ 1.3\ \ (\ H_m/U^2)^{-0.28} \tag{25}$$

where the exponent is $\mu/2$.

In a similar manner to the depth, a general interpolation relationship spanning the strength and shock weakened regimes is given by

$$d/a = K_s\ (Y/\rho U^2)^{-0.28}\ + K_{sw}\ (H_m/U^2)^{-0.28}\ , \tag{26}$$

where for the diameter $K_s = 1.4$ (Eq. 24), and $K_{sw} = 1.3$ (Eq. 25).

Transition from Simple to Complex Craters

The transition from simple to complex craters is the transition from strength-dominated to gravity-dominated craters. A general interpolation relationship for the crater diameter which spans both the gravity and strength regimes is given by

$$d/a = K_s (ga/U^2)^{-0.22} \{ (K_g/K_s)^{-0.22} + [(Y/\rho U^2)\{1 + (K_{sw}/K_s) (Y/\rho H_m)^{0.28} \}^{-1/0.28}] (0.22/0.28) (ga/U^2)^{-1}\}^{-0.22} \quad (27)$$

where for the diameter $K_s = 1.4$ (Eq. 24), and $K_{sw} = 1.3$ (Eq. 25), and $K_g = 4.28$ (Eq. 22). This result is plotted in Figure 10.

The transition diameter, or equivalently, the intersection between the strength and gravity dominated regimes can be readily derived . The transition diameter is obtained by equating Eqs. 22 and 24, and solving for the transition impactor radius. Substituting this radius into Eq. 22 yields the following simple relationship

$$d_t = (K^d_g/K^d_s)^{((2+\mu)/\mu))} Y/\rho g \quad (28)$$

where K^d_g is the gravity proportionality constant in Equation 23 and K^d_g is the strength proportionality constant in Equation 25, and using those numerical values we obtain $(K^d_g/K^d_s)^{((2+\mu)/\mu))} = 8.6$. Note that the transition diameter is directly proportional to the strength and inversely proportional to gravitational acceleration. This result is compared in Fig. 11 to the transition diameters as a function of surface gravity for the terrestrial planets and various satellites [Chapman and McKinnon, 1986; Schenk, 1989].

The transition from simple to complex craters has been studied for some time using static models to predict the slumping of freshly formed craters [Melosh, 1977; Melosh and McKinnon, 1978]. Melosh [1977] found, using a perfectly plastic constitutive relation, that the criterion for stability of freshly formed bowl-shaped craters is given by

$$\rho g D_p/Y = K_m \qquad 5< K_m <10 \quad (29)$$

We will show that Eq. 29 can be cast in the form of Eq. 28 and leads to similar conclusions as those drawn by Melosh. Eq. 29 can be solved for the maximum depth of penetration and that result is used in Eq. 11 to determine the transition impactor radius. Substituting this into Eq.24 for the diameter yields

$$d_t = (K_m K^d_s / K^D_s)\, Y/\rho g \qquad (30)$$

where K^D_S is the strength proportionality constant in Eq. 11.Equating Eq. 28 and 30 gives the following expression for the Melosh constant

$$K_m = K^D_s (K^d_g d_t / K^d_s)^{((2+\mu)/\mu)} \qquad (31)$$

For the numerical values found in our calculational results, we obtain a value of K_m = 8.9, which is in agreement with Melosh's range of values (5=>10).

Shape , Observables, and Inferables

In studying cratering on remote planetary surfaces, the observables are the surface morphology of the craters. In the following section we will relate some of the transient non-observable aspects of the cratering process (e.g. depth of penetration, excavation ....) to the usual observable quantity --- crater diameter.

The maximum transient cavity diameter relative to the final crater diameter in gravity dominated craters is given by dividing Eq. 20 by Eq. 22, which yields

$$d_m/d = 0.5 \qquad (32)$$

and for strength dominated craters, the maximum cavity diameter is equal to the final diameter, except for minor crater rebounding. Notably, the maximum transient diameter is the maximum diameter in this case,

$$dt_m/d = 1 \qquad (33)$$

The maximum crater lip height relative to the crater diameter in gravity dominated craters can be obtained by dividing Eq. 21 by Eq. 22 to get

$$H_\ell/d = 0.12 \qquad (34)$$

The ratio of the time for the crater lip to collapse (t_{lp}) to the time for the crater floor to rebound (t_r) in the gravity dominated regime can be obtained from Figure 4 and is given by

$$t_{lp}/t_r = 2 \tag{35}$$

The depth of penetration relative to the crater diameter for gravity-dominated craters can be obtained by dividing Eq. 9 by Eq. 22, which yields

$$D_p/d = 0.28 \tag{36}$$

and for strength dominated craters by dividing Eq. 11 by Eq. 24, which yields

$$D_p/d = 0.58 \tag{37}$$

In a similar manner,the depth of excavation relative to the crater diameter for gravity dominated craters can be obtained by dividing Eq. 18a by Eq. 22, which yields

$$D_{ex}/d = 0.1 \tag{38}$$

and for strength dominated craters by dividing Eq. 18b by Eq. 24

$$D_{ex}/d = 0.2 \tag{39}$$

Note that the depth of penetration and excavation relative to the crater diameter are a factor of two less in the gravity dominated cases because the crater diameter is larger as a result of the lip collapse and lipwave propagation. The above result for the depth of excavation is compared to field data from terrestrial craters in Fig. 12. The maximum depth of penetration and depth of excavation as a function of crater diameter are plotted for the various planets in Fig. 13. As an example, for craters in the range of 150 km in diameter, which is in the estimated size for the K-T event [Alvarez et al., 1980], the maximum depth of penetration is 42 km while the maximum depth of excavation is ~15 km. Impacts of this magnitude appear to open the possibility of impact-induced volcanism from the mantle.

CONCLUSIONS

The objective of this study was to obtain a quantitative understanding of the cratering process over a broad range of conditions. In accomplishing this objective we

numerically computed the evolution of impact induced flow fields and calculated the time histories of the major measures of crater geometry (e.g. depth, diameter, and lip height) for variations in planetary gravity, material strength, thermal properties and impactor size. The results of these calculations are summarized in Table 2. These results were fit with the scaling laws of Holsapple and Schmidt [1987]. In all of the measures we examined, these scaling laws were found to be in good agreement with the numerical results. From this experience, we expect this agreement to hold in general.

We have described the impact process in terms of four regimes: (1) penetration, (2) inertial, (3) terminal , and (4) relaxation. The scaling laws for each of the first three regimes are given in Table 3. In the penetration regime the depth evolves linearly with time. In the inertial regime, the scaling of the crater geometry is a function of the coupling coefficient (μ) as defined by Holsapple and Schmidt [1987] and was shown by them to be related to the slope of the growth of the depth and diameter in that regime. The results of this paper confirm that relationship.

In studying cratering on remote planetary surfaces, the primary observables are the crater diameter including the diameters of the multiple rings, the presence of central peaks and pits and the relaxed crater depth. We have related several key transient non-observable aspects of the cratering process (e.g. maximum depth of penetration, depth of excavation, and maximum crater lip height) to the crater diameter. For example, the maximum depth of penetration relative to the crater diameter is ~0.58 for strength dominated craters and ~0.28 for gravity dominated craters. This implies that impactors associated with the large basin impacts penetrated deep into the planetary surfaces. In examining the details of the rebounding of the depth in the gravity dominated regime, we found that the initial planetary material layering sequence is reconstructed in the rebound process. This phenomenon thus accounts for apparent contradictions of field data and experiments conducted on the geotechnical centrifuge [Schmidt and Holsapple, 1981], that the impactor did not penetrate very deep because the layering sequence was relatively undisturbed. In a similar manner

to the penetration, the maximum deep of excavation relative to the crater diameter is ~0.1 for gravity dominated craters and ~0.2 for strength dominated; this implies that for impact velocities less than the threshold for significant vaporization, the excavated material can have rather deep origins for large diameter basin-forming craters

The transition from simple bowl shaped craters to complex craters was analyzed. This occurs at the transition from strength to gravity dominated craters. The transition diameter is proportional to $Y/\rho g$ where the proportionality constant is ~8.6. This constant is in the range of values (5-10) found by Melosh [1977] using a gravitational plastic instability model.

Acknowledgments. Research supported under NASA Grant NSG 1953. We appreciate the computational assistance of M. Lainhart and many helpful discussions with K. Holsapple and R. Schmidt. Contribution No. 4859, Division of Geological and Planetary Sciences, California Institute of Technology, Pasadena, 91125.

REFERENCES

Ahrens, T. J., and A. Rubin, Impact-induced tensional failure in rock, *J. Geophys. Res.*, submitted 1992.

Alvarez, L. E., W. Alvarez, F. Asaro, and H. V. Michel, Extraterrestrial cause for the Cretaceous-Tertiary extinction, *Science, 208*, 1095-1108, 1980.

Andrews, R. J., Characteristics of debris from small-scale cratering experiments, in *Impact and Explosion Cratering*, edited by D. J. Roddy, R. O. Pepin and R. B. Merrill, pp. 1089-1100, Pergamon Press, New York, 1977.

Asphaug, E., H. J. Melosh, and E. Ryan, A numerical laboratory for fragmentation studies: Some Insights into collisional processes and outcomes, *LPSC (Abstract), XXII*, 37-38, 1991.

Bjork, R. L., Analysis of the formation of Meteor Crater, Arizona. A preliminary report, *J. Geophys. Res., 66*, 3379-3387, 1961.

Bjorkman, M. D., Dependence of crater melt on impact velocity, *Eos Trans. AGU (abstract), 64*, 747, 1983.

Chapman, C. R., and W. B. McKinnon, Cratering of planetary satellites, in *Satellites*, edited by J. A. Burns and M. S. Matthews, pp. 492-580, 1986.

Frederikson, K., A. Duba, D. J. Milton, and M. S. Balasundaram, Lonar Lake, India: An impact crater in basalt, *Science, 180*, 862-864, 1973.

Gault, D. E., W. L. Quaide, and V. R. Oberbeck, Impact cratering mechanics and structures, in *Shock Metamorphism of Natural Materials*, edited by B. M. French and N. M. Short, pp. 87-100, Mono Press, 1968.

Grieve, R. A. F., P. B. Robertson, and M. R. Dence, Constraints on the formation of ring impact structures, based on terrestrial data in, in *Multi-Ring Basins, Proc. Lunar Planet. Sci.*, vol. 12A, edited by P. H. Schultz and R. B. Merrill, pp. 37-57, Pergamon Press, 1981.

Holsapple, K. A., and R. M. Schmidt, Point-source solutions and coupling parameters in cratering mechanics, *J. Geophys. Res.*, *92*, 6350-6376, 1987.

Housen, K. R., and K. A. Holsapple, On the fragmentation of asteroids and planetary satellites, *Icarus*, *84*, 220-253, 1990.

Kieffer, S. W., *Impact Conditions Required for Melt by Jetting in Silicates. Impact with Explosion Cratering*, Pergamon Press, 1-751, 1976.

Melosh, H. J., Crater modification by gravity: A mechanical analysis of slumping, in *Impact and Explosion Cratering*, edited by D. J. Roddy, R. O. Pepin and R. B. Merrill, pp. 1245-1260, Pergamon Press, New York, 1977.

Melosh, H. J., *Impact Cratering, A Geologic Process*, Oxford University Press, New York, 1-245, 1989.

Melosh, H. J., and W. B. McKinnon, The mechanics of ringed basin formation, *Geophys. Res. Lett.*, *5*, 985-988, 1978.

Offield, T. W., and H. A. Pohn, Deformation at the Decaturville impact structure, Missouri, in *Impact and Explosion Cratering*, edited by D. J. Roddy, R. O. Pepin and R. B. Merrill, pp. 321-341, 1977.

O'Keefe, J. D., and T. J. Ahrens, Impact induced energy partitioning, melting, and vaporization on terrestrial planets, *Proc. Lunar Sci. Conf 8th*, 3357-3374, 1977.

O'Keefe, J. D., and T. J. Ahrens, Large scale impact on the earth with an atmosphere, *Abstract, Lunar and Planetary Science, XIX*, 887-888, 1988.

O'Keefe, J. D., and T. J. Ahrens, The effects of gravity, size, and velocity on the scaling of crater gemetry and the transition from simple to complex craters, *LPSC, XX*, 810-811, 1989.

Roddy, D. J., Large-scale impact and explosion craters: Comparisons of morphological and structural analogs, in *Impact and Explosion Cratering*, edited by D. J. Roddy, R. O. Pepin and R. B. Merrill, pp. 185-246, Pergamon Press, 1977.

Roddy, D. J., S. H. Schuster, M. Rosenblatt, L. B. Grant, P. J. Hassig, and K. N. Kreyenhagen, Computer simulations of large asteroid impacts into oceanic and continental sites---Preliminary results on atmospheric, cratering and ejecta dynamics, *Int. J. Impact Engng.*, *5*, 525-541, 1987.

Schenk, P. M., Crater formation and modification on the icy satellites of Uranus and Saturn: Depth/diameter and central peak occurrence, *J. Geophys. Res.*, *94*, 3813-3832, 1989.

Schmidt, R. M., and K. A. Holsapple, An experimental investigation of transient crater size, *Abstracts, Lunar and Planetary Science, XII*, 934-936, 1981.

Schultz, P. H., and D. E. Gault, Impact ejecta dynamics in an atmosphere: Experimental results and extrapolations, *Geol. Soc. Am. Spec. Paper*, *190*, 152-174, 1981.

Shoemaker, E. M., and R. E. Eggleton, Terrestrial features of impact origin, Proc. Geophys. Lab., Lawrence Radiation Laboratory Cratering Symp., Lawrence Radiation Laboratory Rept. UCRL-6438, pt. 1, paper A27, p., 1961.

Shoemaker, E. M., Impact mechanics at Meteor Crater, Arizona, in *Moon, Meteorites, and Comets*, edited by B. M. Middlehurst and G. P. Kuiper, pp. 301-336, Univ. of Chicago Press, 1963.

Simmons, G., T. Todd, and H. Wang, The 25-km discontinuity: Implications for Lunar History, *Science*, *182*, 158-161, 1973.

Thompson, S. L., Sandia National Labs, Albuquerque, N.M., SAND 77-1339, p., 1979.

Table 1. Scope of Parameters Studied for Impact of Silicate Projectile on a Planetary Halfspace.

Parameter	Symbol	Values Employed	Units
impact velocity	U	12	km/sec
planetary gravity	g	$0,1,10^2,10^4,10^6$	ge ($980 cm/s^2$)
density	ρ	2.7	g/cm^3
bulk modulus	E	7.6×10^{11}	$dynes/cm^2$
Gruneisen coefficient	γ	2.0	—
melt enthalpy	H_m	1.1×10^{10}	ergs/g
vaporization enthalpy	H_{vap}	1.2×10^{11}, 1.2×10^{12}, 8.0×10^{12}	ergs/g
yield strength	Y	0,0.24,2.4,5.6, 24, 28,140, 240,2400	kbar
inverse Froúde Number	ga/U^2	$0,3.4\times10^{-7},3.4\times10^{-5},3.4\times10^{-3},0.34$	—
inverse Cauchy Number	$Y/\rho U^2$	$0, 7.2\times10^{-5},7.2\times10^{-4},7.2\times10^{-3},0.036$	—
melt number	H_m/U^2	7.6×10^{-3}	
vaporization number	H_{vap}/U^2	0.08, 0.8, 1.2	—

Table 2. Normalized Crater Diameter and Depth, versus, τ for different values of ga/U^2, and $Y/\rho U^2$. The impact velocity, U, was 12 km/s except where indicated.

ga/U^2	$Y/\rho U^2$	d/a	D/a	τ
0	0.0		0.43	0.870
"	0.0		1.07	2.140
"	0.0		1.53	3.119
0 (U=10km/s)[a]	0.0		0.2	0.4
"	0.0		0.8	1.6
"	0.0		2.0	5.0
"	0.0		3.0	12.0
"	0.0		4.0	16.0
0 (U=50km/s)[a]	0.0		0.4	0.8
"	0.0		1.0	2.0
"	0.0		2.0	4.0
"	0.0		2.6	6.0
"	0.0		4.0	19.0
"	0.0		5.2	50.0
0 (U=100km/s)[a]	0.0		0.2	0.41
"	0.0		1.0	2.00
"	0.0		2.0	4.00
"	0.0		2.6	6.00
"	0.0		4.0	20.00
"	0.0		5.0	40.00
"	0.0		6.0	75.00
"	0.0		7.0	105.00
"	0.0		8.0	130.00
"	0.0		9.5	200.00
3.41×10^{-7}	1.4×10^{-3}	3.400	1.65	3.18
"	1.4×10^{-3}	5.100	3.00	9.28
"	1.4×10^{-3}	5.700	3.35	12.28
"	1.4×10^{-3}	6.500	3.75	16.50
"	1.4×10^{-3}	6.500	3.75	16.50
"	1.4×10^{-3}	6.600	3.95	18.50
"	1.4×10^{-3}	7.400	4.40	23.30
"	1.4×10^{-3}	7.800	4.75	29.64
"	1.4×10^{-3}	8.800	5.15	41.00
"	1.4×10^{-3}	9.000	5.20	55.90
"	1.4×10^{-3}	9.000	5.10	75.40
"	1.4×10^{-3}	9.000	5.10	94.00
	1.4×10^{-3}	9.000	5.00	113.00
3.41×10^{-7}	7.2×10^{-3}	3.500	1.700	3.480
"	7.2×10^{-3}	4.500	2.700	7.700

Table 2. Normalized Crater Diameter and Depth, versus, τ for different values of ga/U^2, and $Y/\rho U^2$. The impact velocity, U, was 12 km/s except where indicated.(continued)

ga/U^2	$Y/\rho U^2$	d/a	D/a	τ
"	7.2×10^{-3}	5.000	3.000	10.560
"	7.2×10^{-3}	5.500	3.500	14.800
"	7.2×10^{-3}	5.700	3.700	17.600
"	7.2×10^{-3}	6.000	3.750	22.100
"	7.2×10^{-3}	6.000	3.600	26.400
"	7.2×10^{-3}	5.700	3.400	30.480
"	7.2×10^{-3}	5.600	3.200	34.300
"	7.2×10^{-3}	5.400	2.800	37.400
3.41×10^{-7}	3.6×10^{-2}	3.300	1.750	3.360
"	3.6×10^{-2}	4.350	2.900	8.900
"	3.6×10^{-2}	4.600	3.100	13.300
"	3.6×10^{-2}	4.600	2.950	17.200
"	3.6×10^{-2}	4.500	2.700	21.020
"	3.6×10^{-2}	4.200	2.500	24.400
"	3.6×10^{-2}	4.000	2.450	26.800
"	3.6×10^{-2}	3.800	2.300	29.500
"	3.6×10^{-2}	2.100	2.200	34.080
"	3.6×10^{-2}	1.000	1.500	49.600
3.41×10^{-5}	0.0		0.37	0.825
"	0.0		1.16	2.350
"	0.0		2.17	5.590
"	0.0		2.60	7.700
"	0.0		1.67	3.600
"	0.0		3.02	10.100
"	0.0		3.53	14.180
"	0.0		4.05	19.000
"	0.0		4.42	24.000
3.41×10^{-3}	0.0		0.40	0.825
"	0.0		1.90	4.480
"	0.0		2.63	7.890
"	0.0		3.25	13.279
"	0.0		4.10	22.770
"	0.0		4.20	32.000
"	0.0		3.10	41.200
"	0.0		1.40	50.600
"	0.0		1.20	2.360
"	0.0		4.10	27.600
"	0.0		3.45	36.800
3.41×10^{-3}	6.2×10^{-5}		0.75	1.550
"	6.2×10^{-5}		0.40	0.854
"	6.2×10^{-5}		1.20	2.370

Table 2. Normalized Crater Diameter and Depth, versus, τ for different values of ga/U^2, and $Y/\rho U^2$. The impact velocity, U, was 12 km/s except where indicated.(continued)

ga/U^2	$Y/\rho U^2$	d/a	D/a	τ
"	6.2×10^{-5}		1.50	3.090
"	6.2×10^{-5}		1.60	3.370
"	6.2×10^{-5}		1.70	3.640
"	6.2×10^{-5}		2.00	5.200
"	6.2×10^{-5}		2.30	6.070
"	6.2×10^{-5}		0.10	0.200
"	6.2×10^{-5}		2.70	8.350
"	6.2×10^{-5}		2.50	7.200
"	6.2×10^{-5}		2.90	9.660
"	6.2×10^{-5}		3.20	12.690
"	6.2×10^{-5}		3.60	17.100
"	6.2×10^{-5}		3.80	21.900
"	6.2×10^{-5}		3.90	27.800
"	6.2×10^{-5}		3.65	35.400
"	6.2×10^{-5}		3.00	42.600
"	6.2×10^{-5}		2.00	50.400
3.41×10^{-3}	6.2×10^{-4}		0.50	0.907
"	6.2×10^{-4}		1.10	2.052
"	6.2×10^{-4}		1.70	3.280
"	6.2×10^{-4}		2.15	4.776
3.41×10^{-3}	6.2×10^{-3}		0.50	0.934
"	6.2×10^{-3}		1.22	2.324
"	6.2×10^{-3}		1.85	3.710
"	6.2×10^{-3}		2.35	5.560
"	6.2×10^{-3}		2.55	7.040
"	6.2×10^{-3}		3.00	10.150
"	6.2×10^{-3}		3.35	15.090
"	6.2×10^{-3}		3.30	20.020
"	6.2×10^{-3}		2.20	43.200
"	6.2×10^{-3}		1.85	50.850
"	6.2×10^{-3}		3.00	27.600
"	6.2×10^{-3}		2.50	35.470
3.4×10^{-2}	0	1.250	1.400	21.670
"	0	0.900	0.600	28.800
"	0	0.700	0.200	33.600
"	0	0.250	0.100	37.700
"	0	2.450	0.100	42.960
"	0	4.100	0.100	46.560
3.4×10^{-2}	6.2×10^{-5}	2.000	0.400	0.828
"	6.2×10^{-5}	2.750	1.100	2.120

Table 2. Normalized Crater Diameter and Depth, versus, τ for different values of ga/U^2, and $Y/\rho U^2$. The impact velocity, U, was 12 km/s except where indicated.(continued)

ga/U^2	$Y/\rho U^2$	d/a	D/a	τ
"	6.2×10^{-5}	3.300	1.700	3.380
"	6.2×10^{-5}	3.550	2.000	4.580
"	6.2×10^{-5}	3.850	2.350	6.020
"	6.2×10^{-5}	4.100	2.450	7.990
"	6.2×10^{-5}	4.250	2.450	10.200
"	6.2×10^{-5}	4.850	2.200	13.700
"	6.2×10^{-5}	6.600	1.950	17.600
"	6.2×10^{-5}	8.350	1.550	21.300
"	6.2×10^{-5}	8.600	1.150	24.900
"	6.2×10^{-5}	8.100	0.650	28.500
"	6.2×10^{-5}	8.200	0.500	31.400
"	6.2×10^{-5}	8.600	0.350	34.000
"	6.2×10^{-5}	8.600	0.300	34.800
3.41×10^{-2}	6.2×10^{-4}	5.200	2.200	13.750
"	6.2×10^{-4}	9.150	1.550	21.300
"	6.2×10^{-4}	9.100	0.800	28.560
"	6.2×10^{-4}	9.100	0.400	34.100
"	6.2×10^{-4}	9.100	0.350	34.800
"	6.2×10^{-4}	9.100	0.200	38.920
"	6.2×10^{-4}	10.000	0.300	44.880
"	6.2×10^{-4}		0.400	49.920
3.4×10^{-2}	6.2×10^{-3}	2.700	1.350	2.920
"	6.2×10^{-3}	2.950	2.150	5.600
"	6.2×10^{-3}	4.400	2.350	8.320
"	6.2×10^{-3}	4.600	2.350	10.200
"	6.2×10^{-3}	5.050	2.150	12.800
"	6.2×10^{-3}	5.550	2.000	14.400
"	6.2×10^{-3}	6.500	1.850	16.200
"	6.2×10^{-3}	7.500	1.600	17.900
"	6.2×10^{-3}	8.200	1.400	19.600
"	6.2×10^{-3}	9.400	0.800	23.800
3.4×10^{-2}	6.2×10^{-2}	4.850	2.050	13.890
"	6.2×10^{-3}	5.100	1.850	15.840
"	6.2×10^{-3}	5.300	1.650	17.760
"	6.2×10^{-3}	7.500	0.850	24.960
"	6.2×10^{-3}	8.100	0.100	32.640
3.4×10^{-2}	6.2×10^{-1}	3.000	1.350	2.610
"	6.2×10^{-1}	3.350	1.750	3.690
"	6.2×10^{-1}	3.800	2.250	6.450

Table 2. Normalized Crater Diameter and Depth, versus, τ for different values of ga/U^2, and $Y/\rho U^2$. The impact velocity, U, was 12 km/s except where indicated.(continued)

ga/U^2	$Y/\rho U^2$	d/a	D/a	τ
"	6.2×10^{-1}	4.000	2.400	8.640
"	6.2×10^{-1}	3.950	2.350	9.980
"	6.2×10^{-1}	3.950	2.350	10.500
"	6.2×10^{-1}	4.150	2.200	12.600
"	6.2×10^{-1}	4.200	1.950	18.000
3.4×10^{-2}	6.2	3.200	1.450	2.660
"	6.2	3.800	2.400	6.766
"	6.2	4.050	2.400	9.040
"	6.2	4.150	2.350	11.400
"	6.2	4.200	2.250	12.900
"	6.2	4.050	2.000	16.300
0.341	0.0	2.1	0.40	0.765
"	0.0	2.8	1.10	2.010
"	0.0	2.3	1.50	4.080
"	0.0	5.0	1.35	5.220
"	0.0	5.8	1.10	5.970
"	0.0	2.6	1.50	3.500
"	0.0	2.0	1.40	4.480
"	0.0	6.8	1.10	7.050
"	0.0	2.4	1.50	3.900
"	0.0	2.3	1.45	4.180
	0.0	4.0	1.30	4.750
	0.0	5.3	1.25	5.678
0.341	6.2×10^{-5}		0.38	0.761
"	6.2×10^{-5}		0.68	1.290
"	6.2×10^{-5}		0.90	1.700
"	6.2×10^{-5}		1.15	2.130
"	6.2×10^{-5}		1.30	2.490
"	6.2×10^{-5}		1.35	2.950
"	6.2×10^{-5}		1.43	3.400
"	6.2×10^{-5}		1.50	2.880

(a) Time history taken from Holsapple & Schmidt (1987).

TABLE 3. SUMMARY OF CRATER SCALING FORMULA

Regime	Formula	Proportionality Constant (K)	Exponent	Comments
Penetration Regime				
Depth Evolution	$D/a = 0.5(Ut/a)$	0.5	1	Independent of material properties
Depth transition to inertial regime	$Ut/a=5.1$	—		
Diameter Evolution		—		
Diameter transition to inertial regime	$Ut/a=2$	1.3	0.78	$1<(Ut/a)<5.1$
Diameter/depth evolution	$d/D=K(Ut/a)$			
Inertial Regime				
Depth Evolution	$D/a=K(Ut/a)^s$	1.3	0.36	Independent of material properties
Coupling coefficient	$\mu = s/(1-s)$	0.56	—	Slope of growth, s, determines the value of $\mu = s/(1-s)$ which, in turn, determines the exponents for all regimes (Holsapple and Schmidt, 1987)
Transition to terminal (g)*	$Ut/a=K(ga/U^2)^{-(1+\mu)(2+\mu)}$	0.92	0.61	
Transition to terminal (Y)+	$Ut/a=K(Y/\rho U^2)^{-(1+\mu)/2}$	0.33	0.78	
Maximum depth of penetration (g)	$D_p/a = K\,(ga/U^2)^{-\mu/(2+\mu)}$	1.2	0.22	
Maximum depth of penetration (Y)	$D_p/a=K(Y/\rho U^2)^{-\mu/2}$	0.84	0.28	
Maximum depth penetration(Y_{sw})++	$D_p/a=K(H_m/U^2)^{-\mu/2}$	0.70	0.28	

TABLE 3. SUMMARY OF CRATER SCALING FORMULA (continued)

Penetration Regime	Formula	Constant (K)	Exponent	Comments
Diameter Evolution	$d/a=K\,(Ut/a)^{s}$	2.0	0.36	Crater grows until
Maximum cavity diameter (g)	$d_m/a=K(ga/U^2)^{-\mu/(2+\mu)}$	2.1	0.22	arrested by strength
Maximum diameter (Y)	$d_m/a=K(Y/\rho U^2)^{-\mu/2}$	1.4	0.28	and/or gravitational
Maximum diameter (Y_{SW})	$d_m/a=K(H_m/U^2)^{-\mu/2}$	1.3	0.28	forces
Transition time to terminal (g)	$Ut/a=K(ga/U^2)^{-(1+\mu)(2+\mu)}$	1.80	0.61	
Transition time to terminal (Y)	$Ut/a=K(Y/\rho U^2)^{-(1+\mu)(2+\mu)}$	0.33	0.78	
Maximum lip height (g)	$H_\ell/a=K(ga/U^2)^{-\mu/(2+\mu)}$	0.53	0.22	
Diameter/Depth Evolution	$d/D=K(Ut/a)^{-1/(1+\mu)}$	4.0	0.64	$1<(Ut/a)<5.1$
	$d/D=K$	1.6		$5.1<(Ut/a<)t_{mp}$
Terminal Regime				
Transition diameter from simple to complex craters	$d_t=K(Y/\rho g)$	8.6	—	In strength dominated regime
Maximum diameter (g)	$d_m/a = K\,(ga/U^2)^{-\mu/(2+\mu)}$	4.28	0.22	only minor elastic rebounding . In
Maximum transient diameter/ diameter (g)	$d_m/d = 0.5$			gravity dominated regime crater
Maximum transient diameter/ diameter (Y)	$d_m/d = 1.0$			evolves until
Maximum lip height/diameter	$H_\ell\ d = 0.12$			arrested by strength
Depth of penetration/diameter (g)	$D_p/d = 0.28$			forces
Depth of penetration/diameter (Y)	$D_p/d = 0.58$			
Depth of excavation/diameter (g)	$D_{ex}/d = 0.1$			
Depth of excavation/diameter (Y)	$D_{ex}/d = 0.2$			

* (g) Regime indicated is gravity dominated
+ (Y) Regime indicated is strength dominated
++ Y_{SW} Regime indicated is shock wave degraded strength dominated

Figure 1. Simple bowl shaped crater Flow field for the impact of a silicate projectile on a silicate halfspace. The flow field is in the strength dominated regime with $ga/U^2 = 3.7 \times 10^{-7}$ and $Y/\rho U^2 = 1.4 \times 10^{-3}$. The velocity field is shown on the left side with the scale shown at the top. On the right hand are the trajectories of tracer particles placed at various depths. The panels represent dimensionless times of 3.19, 9.29 and 16.6. This is representative of a simple bowl shaped crater.

Figure 2. Complex crater Velocity and deformation history fields for the impact of a silicate projectile on a silicate halfspace. the flow field is gravity dominated at late times with $ga/U^2 = 3.4 \times 10^{-2}$ and $Y/\rho U^2 = 6.2 \times 10^{-3}$. The velocity field is shown on the left side with the scale at the top. On the right side are the trajectories of tracer particles placed at various depths. The panels represent dimensionless times of 5.57, 8.32, 10.2, 12.8, 14.4, 17.9, and 19.7.

Figure 3. Dimensionless depth versus dimensionless time for the penetration, and inertial, terminal and relaxation regimes for different values of ga/U^2 and $Y/\rho U^2$.

Figure 4. Temporal evolution of the dimensionless depth of penetration (D/a) and crater diameter (d/a) for a fixed value of inverse Froúde number (ga/U^2=0.034), and various values of $Y/\rho ga$.

Figure 5. Dimensionless maximum depth of penetration (D_p/a) and diameter (d/a) as a function inverse Froúde number (ga/U^2). Slope corresponds to - $\mu/(2+\mu)$ for gravity scaling. Symbols are results for different calculations.

Figure 6. Temporal evolution of dimensionless depth (D/a) and diameter (d/a) in the strength dominated region.

Figure 7. Dimensionless maximum depth of penetration (D_p/a) and diameter (d/a) as a function of inverse Cauchy number ($Y/\rho U^2$). The slope is -0.28=-$\mu/2$ and corresponds to strength scaling. The change in slope is a result of melting and shock weakening. Symbols represent different calculations for a fixed value of Froúde number (ga/U^2=0.034) for various values of the melt number (H_m/U^2).

Figure 8. Dimensionless crater diameter (d/a) as a function of inverse Cauchy number ($Y/\rho U^2$) in the strength dominated regime (see Figure 10).

Figure 9. Effective strength as a function of weakening energy.

Figure 10. Dimensionless crater diameter as a function of inverse Froúde number (ga/U^2) for various values of inverse Cauchy number ($Y/\rho U^2$). Slope corresponds to gravity scaling.

Figure 11. Crater transition diameter from simple to complex craters as a function of planetary surface gravity. Slope corresponds to scaling law of Eq. 28.

Figure 12. Depth of excavation of planetary material (D_{ex}) divided by the crater diameter (d) as a function of crater diameter for terrestrial craters. Calculation results indicated by solid line. (a) sand, Gault et al., 1968; (b) sand, Andrews, 1976; (c) 500 ton TNT, Roddy, 1976; (d) Jangle U, Shoemaker, 1963; (e) Teapot Ess, Shoemaker, 1963; (f)

Odessa, Shoemaker and Eggleston, 1961; (g) Lonar Lake, Fredriksson et al., 1973; (h) Decaturville, Offield and Pohn, 1976.

Figure 13. Maximum depth of penetration (D_p) and excavation (D_{ex}) as a function of crater diameter for various planets and satellites. Vertical lines delineate the transition from strength to gravity scaling.

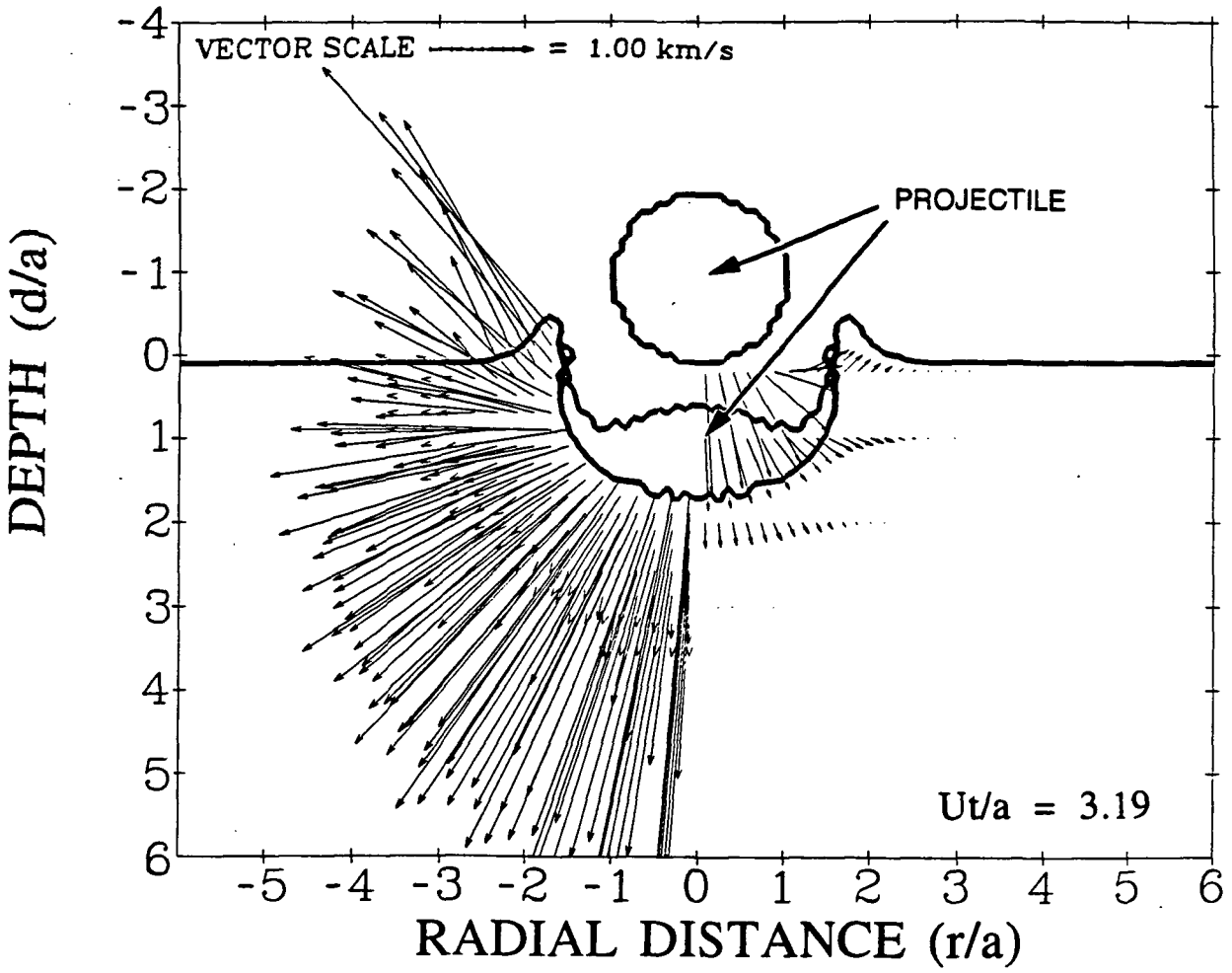

mike ** Sat Oct 26 16:18:29 1991

TJA92016MFD

1A

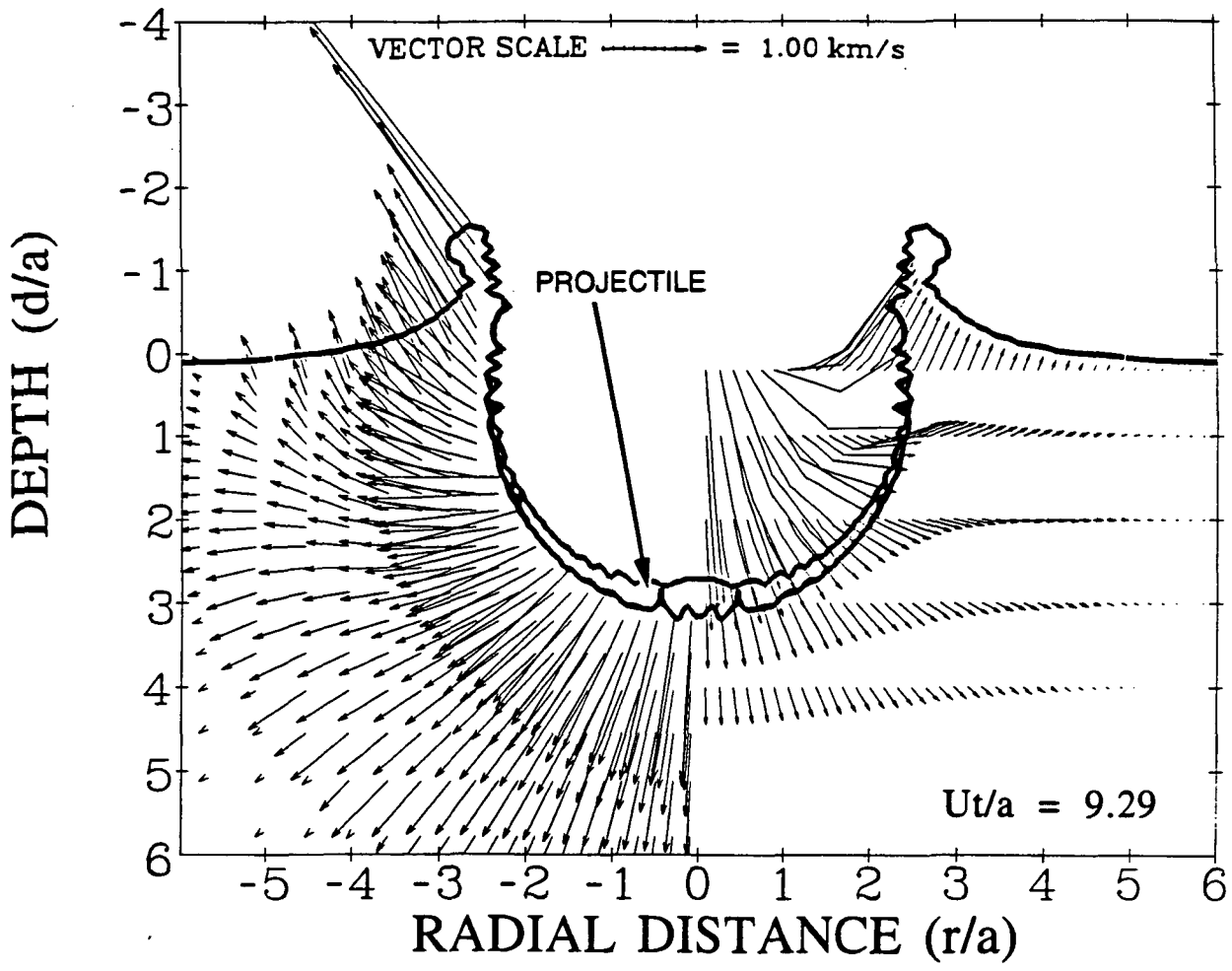

mike ** Sat Oct 26 16:19:15 1991

TJA92017MFD

16

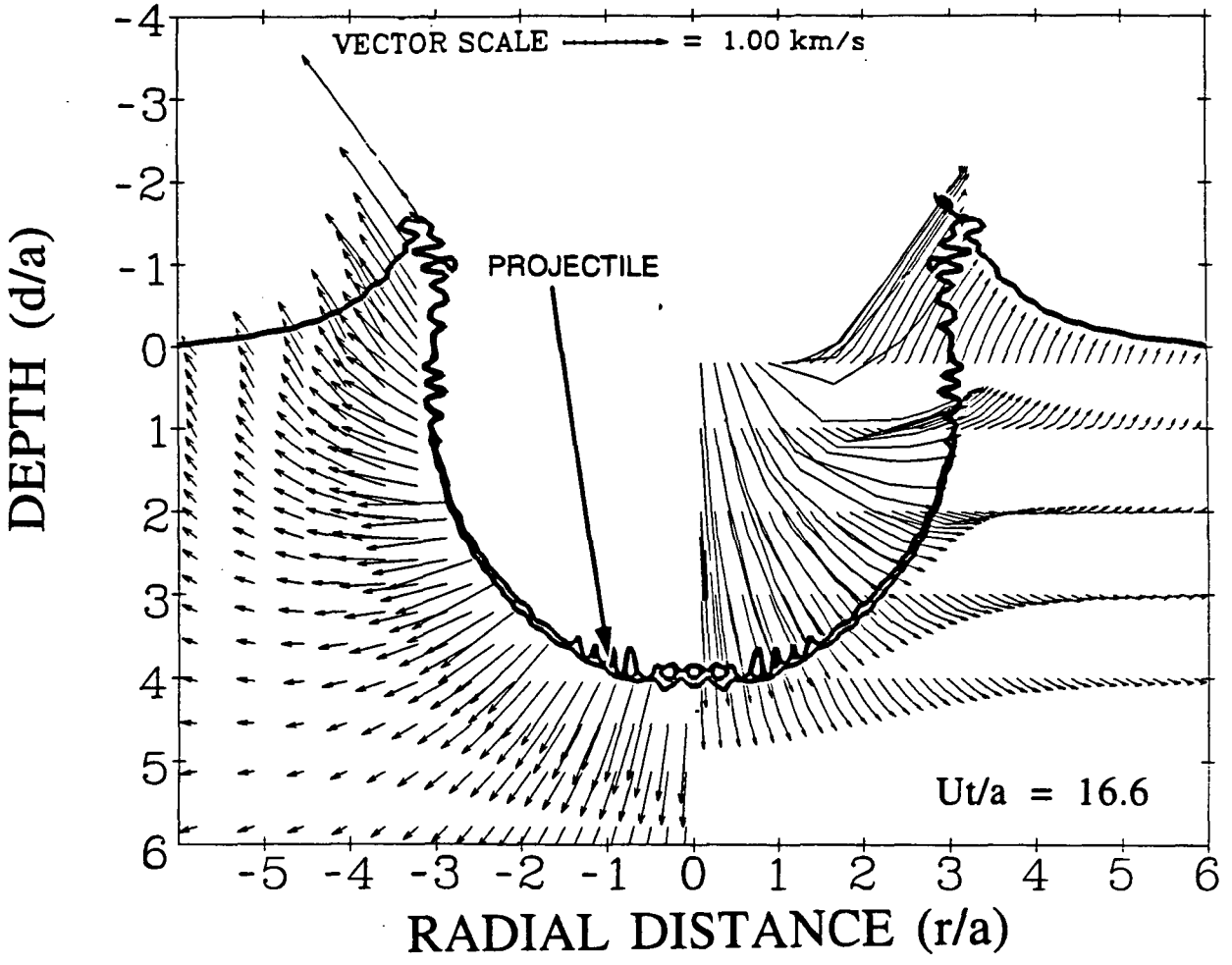

TJA92018MFD

mike ** Sat Oct 26 16:25:47 1991

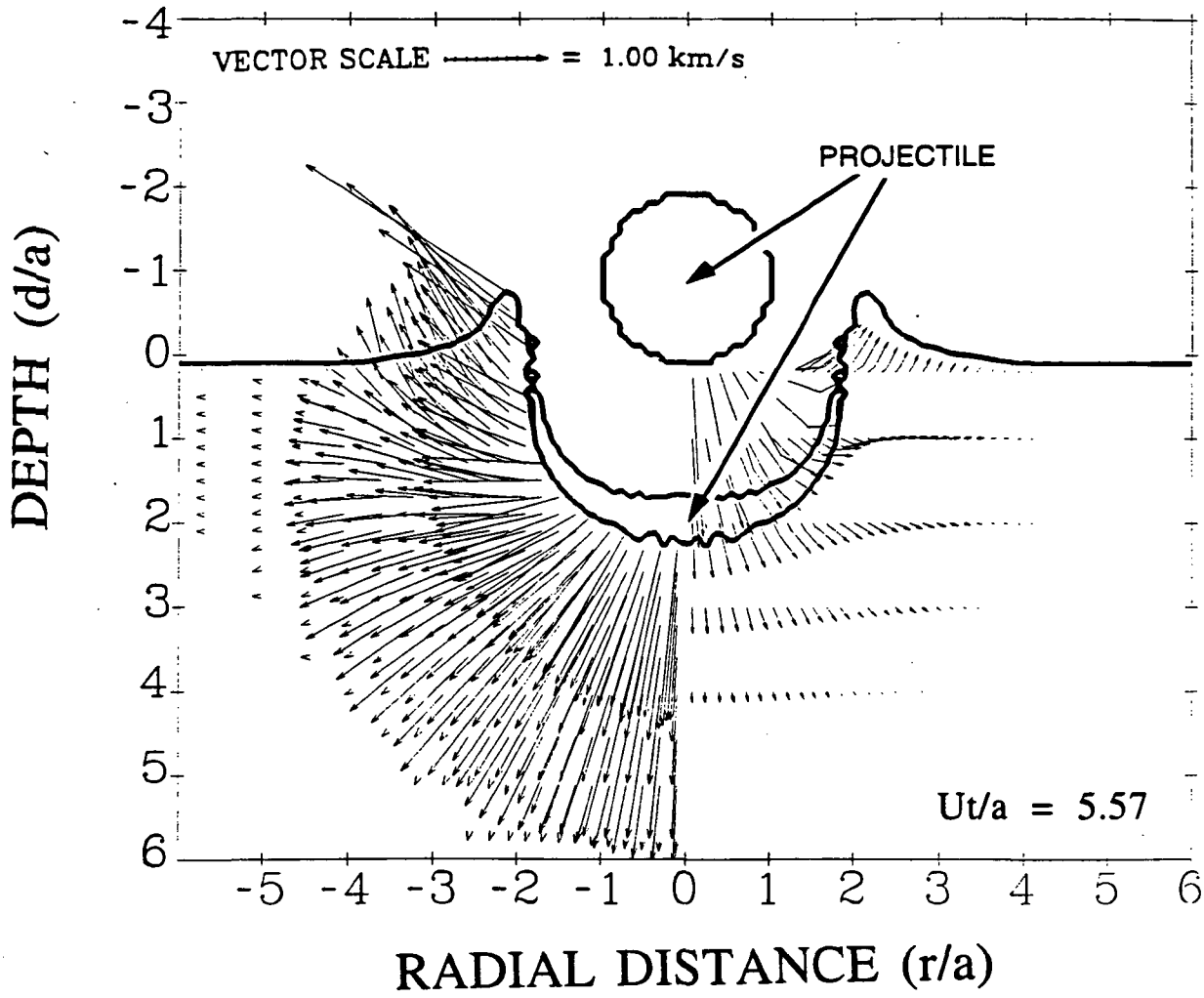

TJA92019MFD

2a

Tue Nov 24 20:23:34 1992

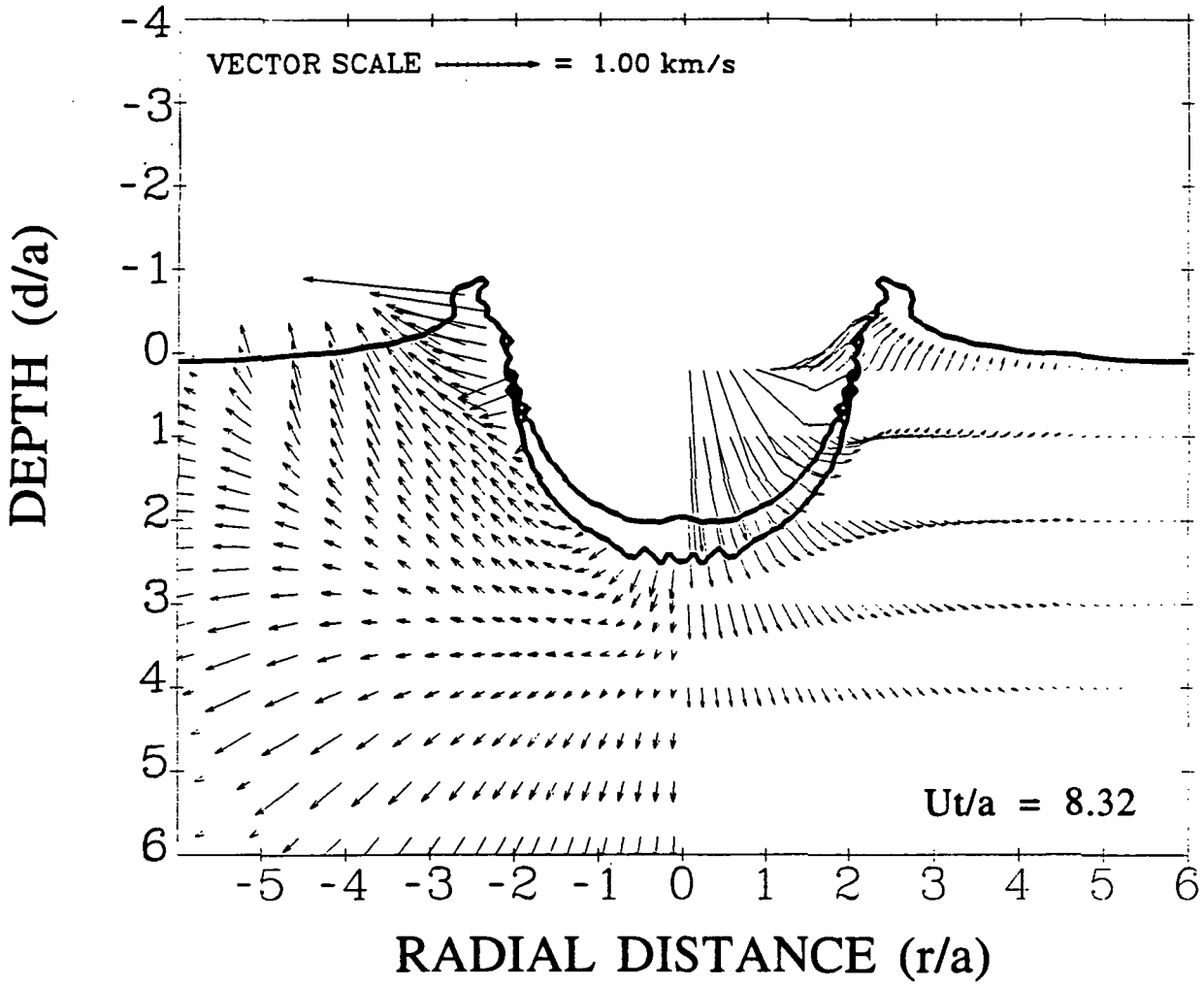

TJA92020MFD

2b

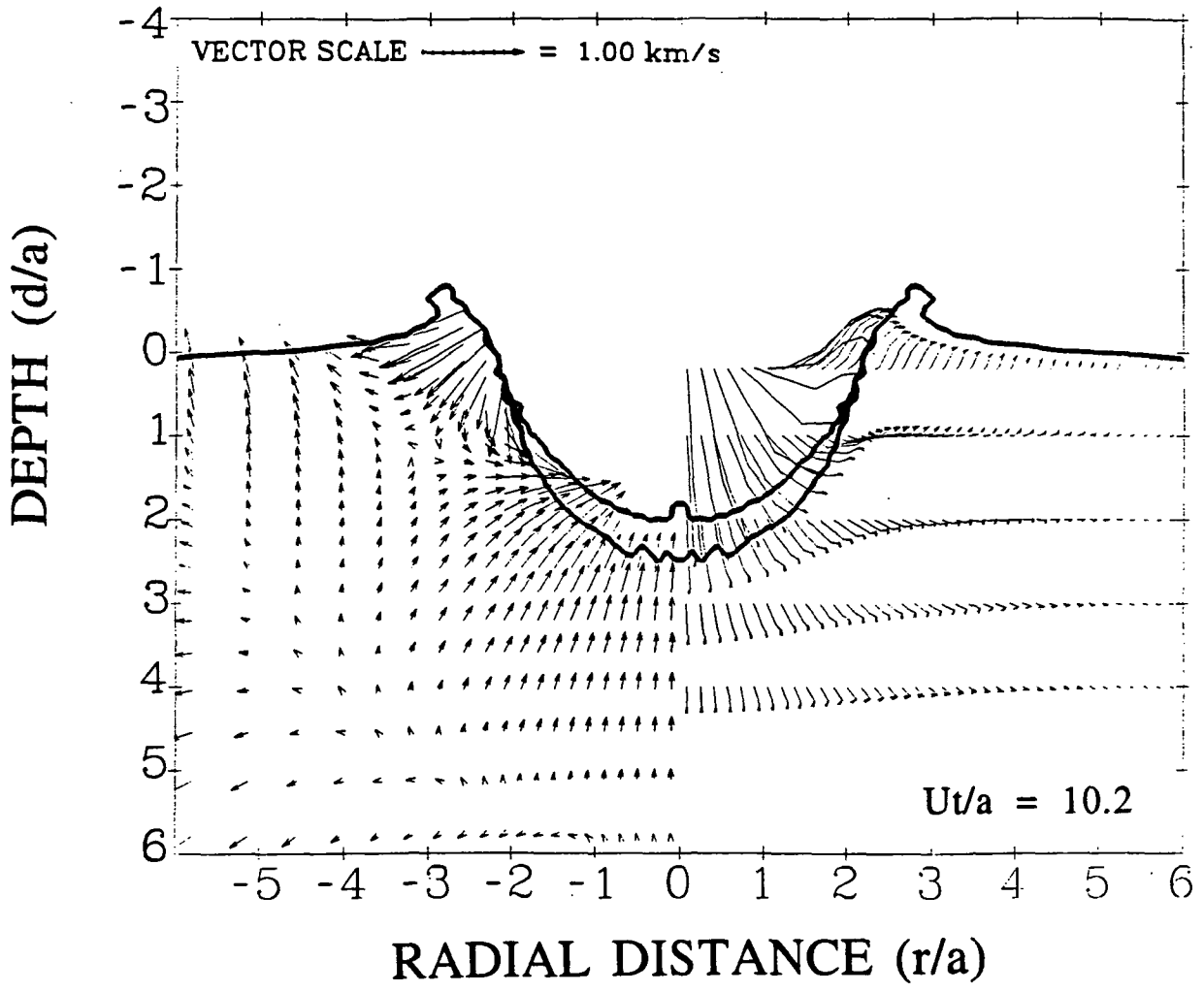

TJA92021MFD

Sun Nov 24 20:25:12 1991

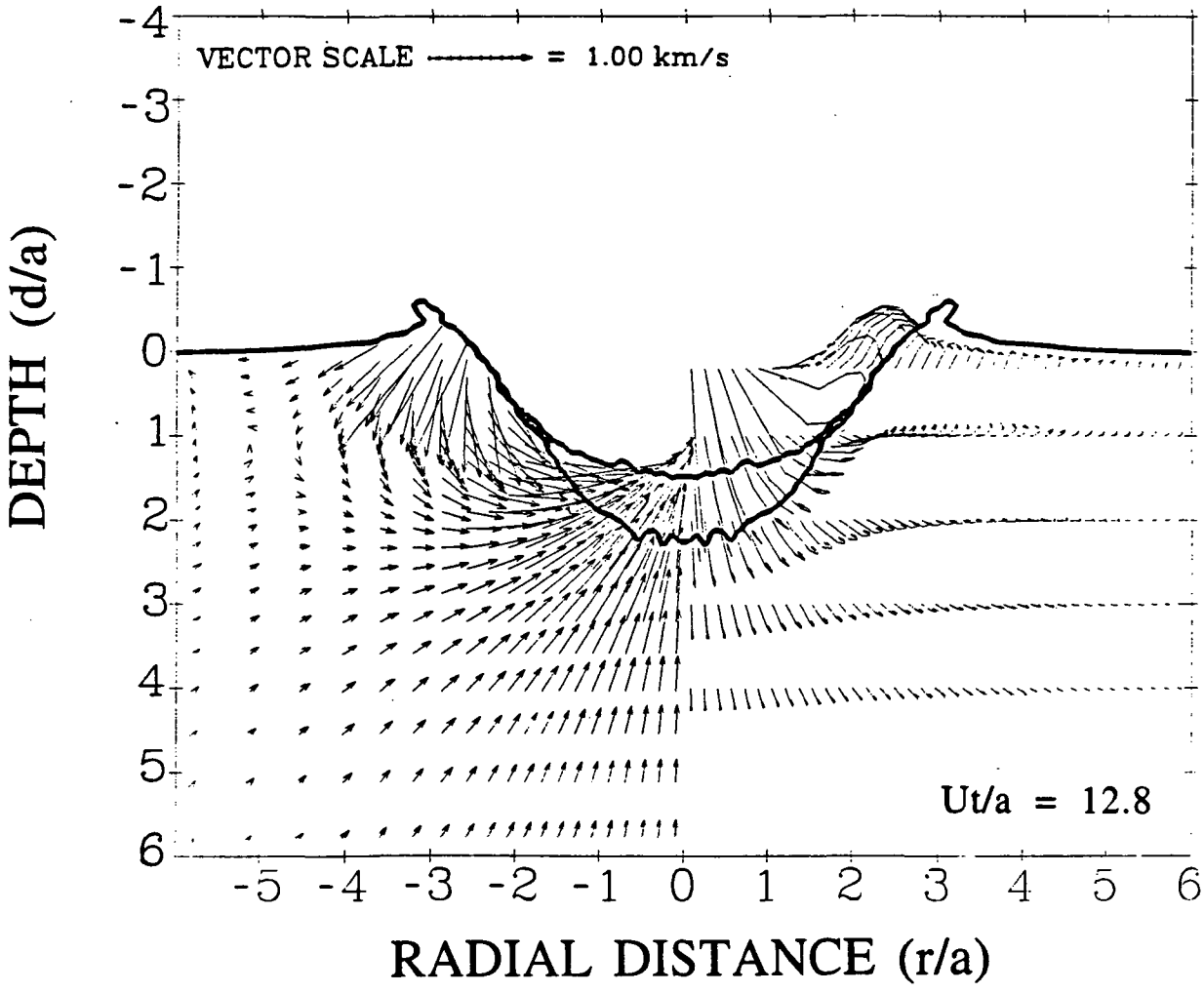

TJA92022MFD

Tue Nov 24 20:25:57 1992

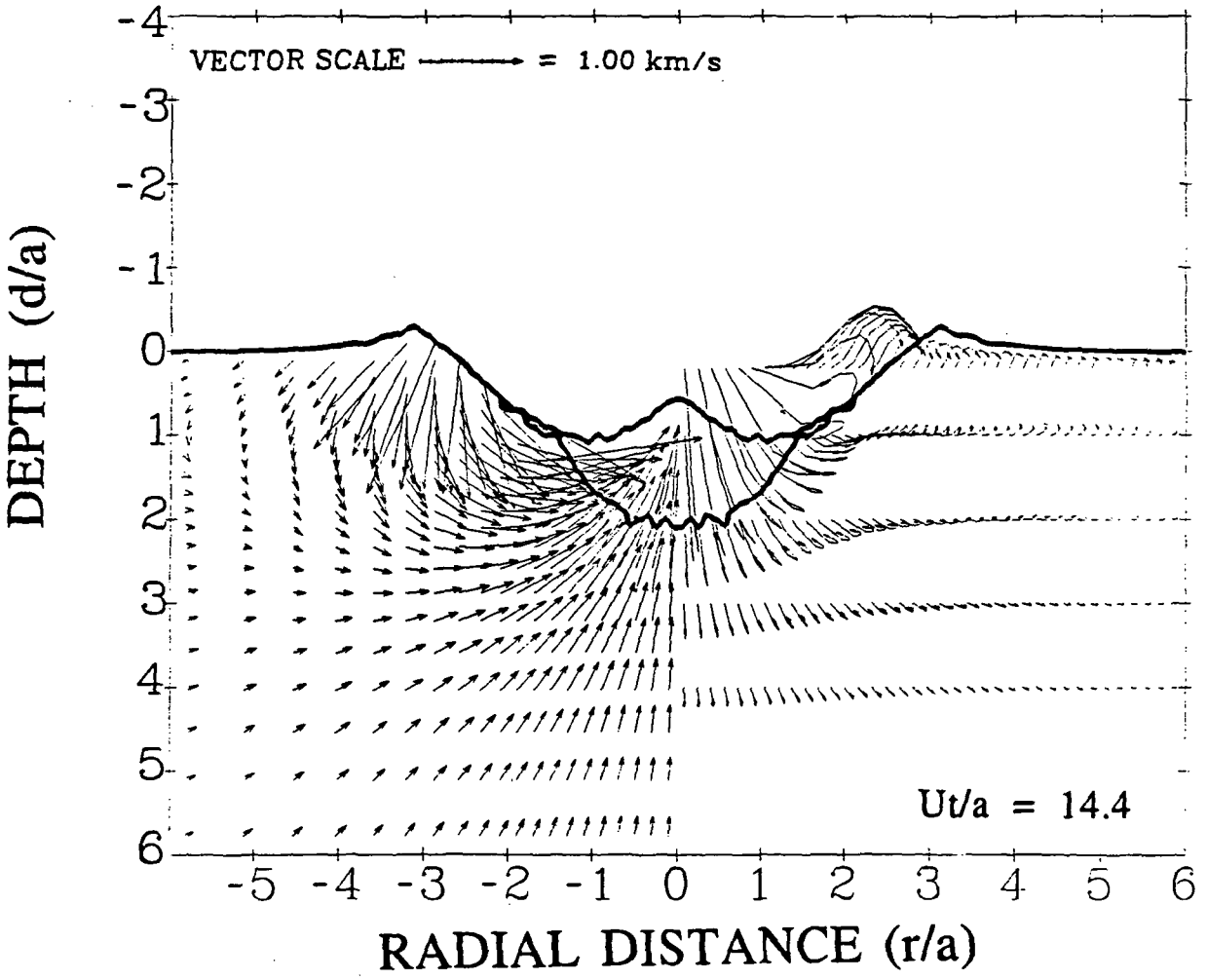

TJA92023MFD

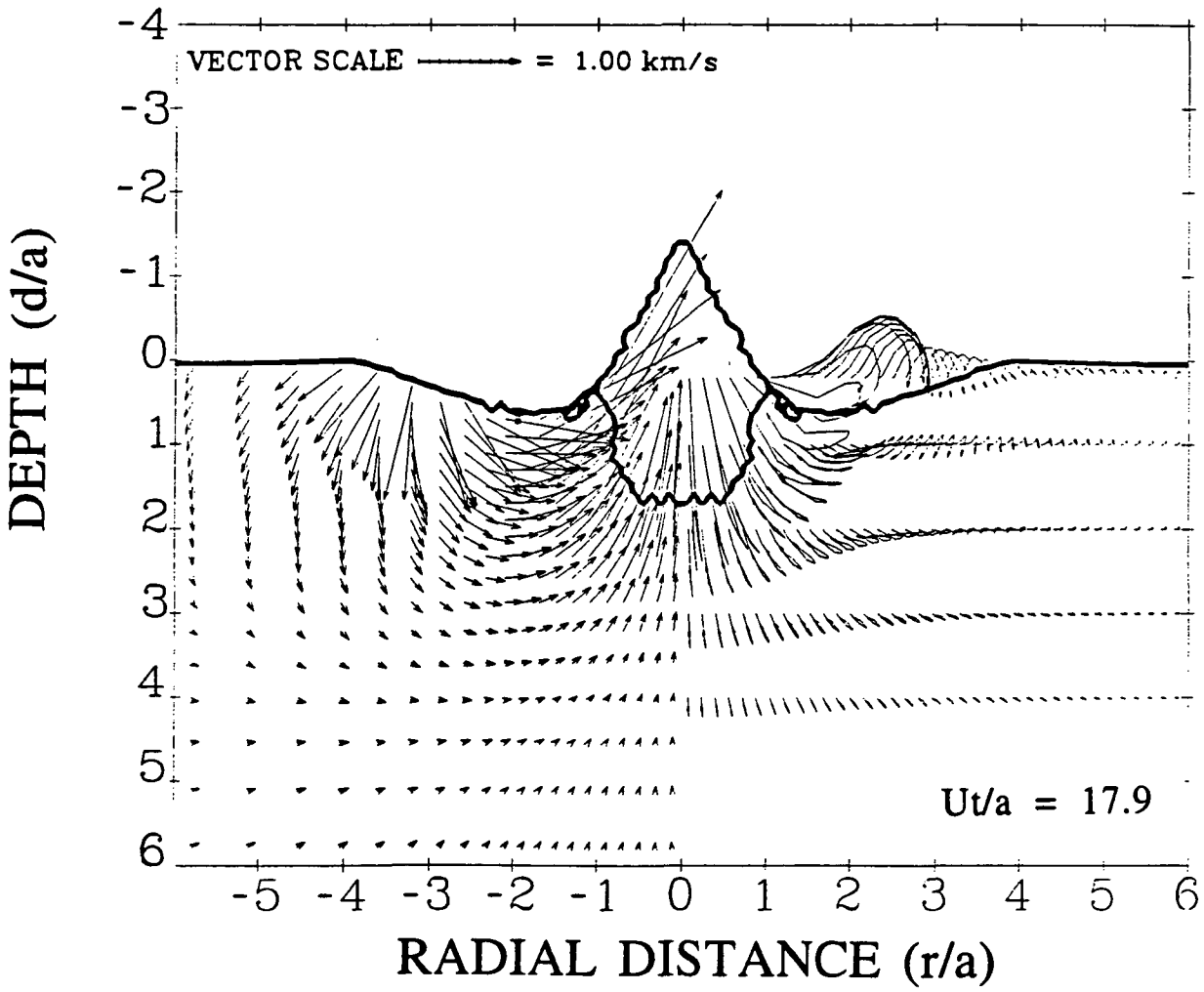

TJA92024MFD

mike ** Sun Nov 24 20:28:21 1991

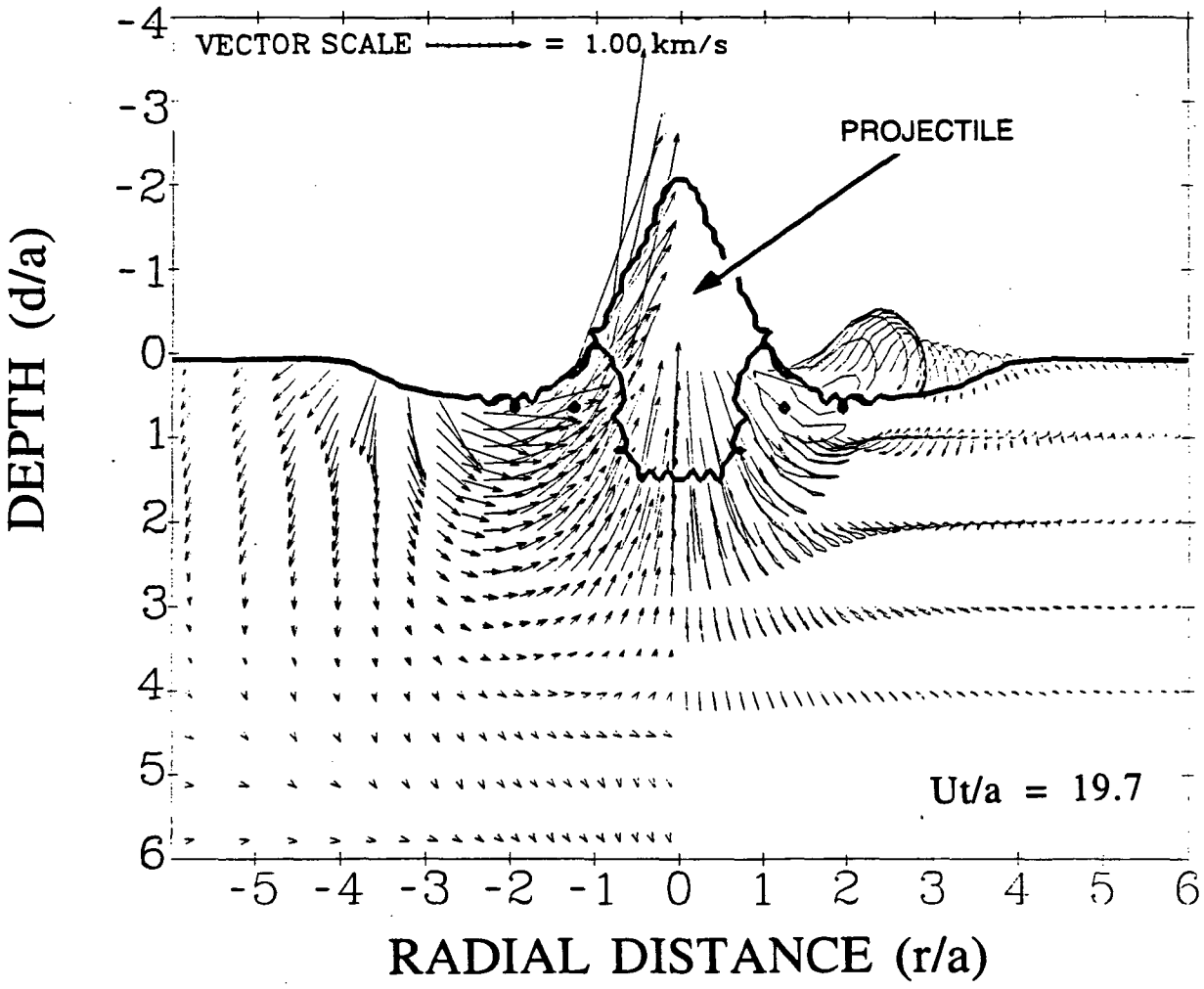

TJA92025MFD

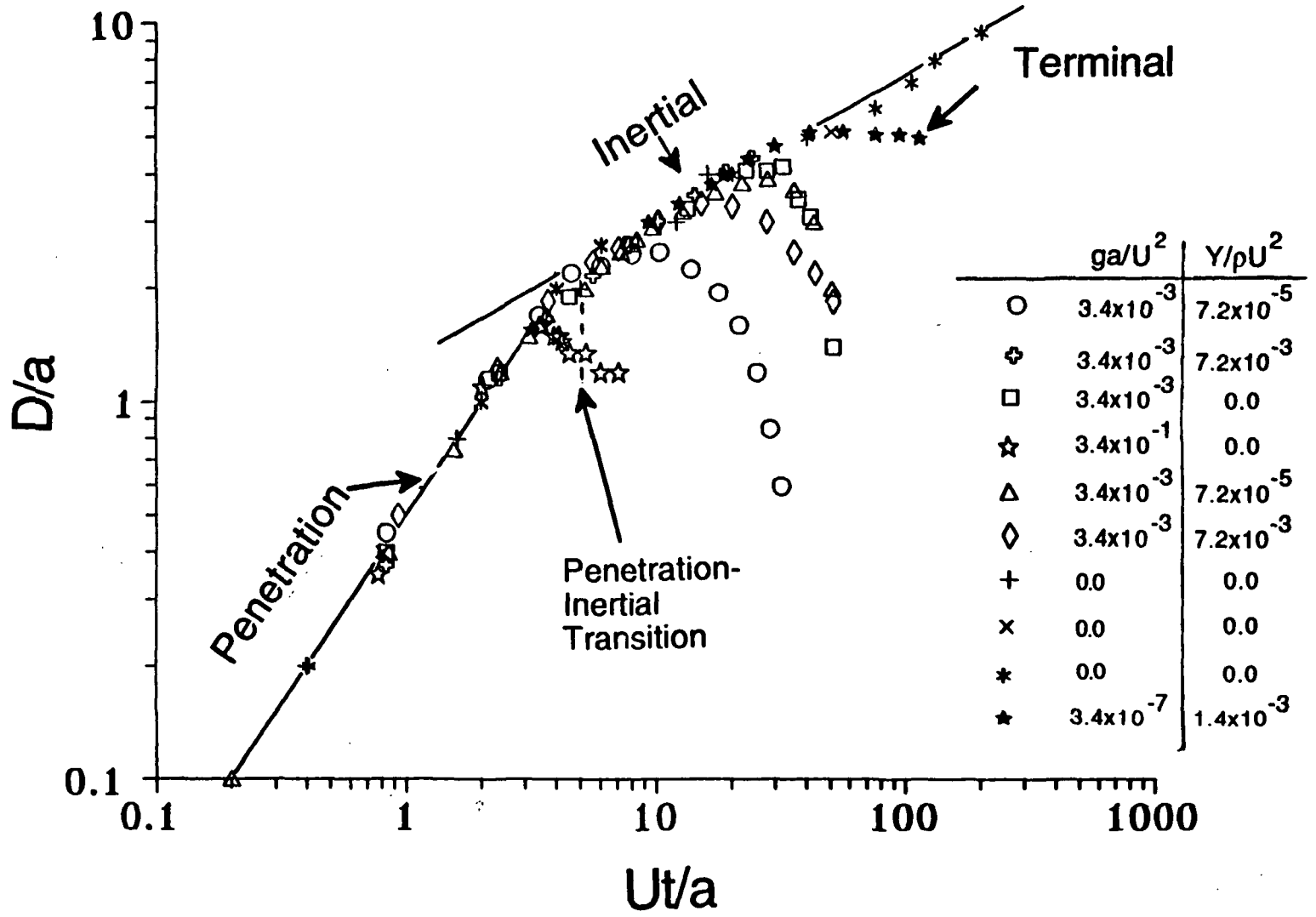

TJA92026SFD

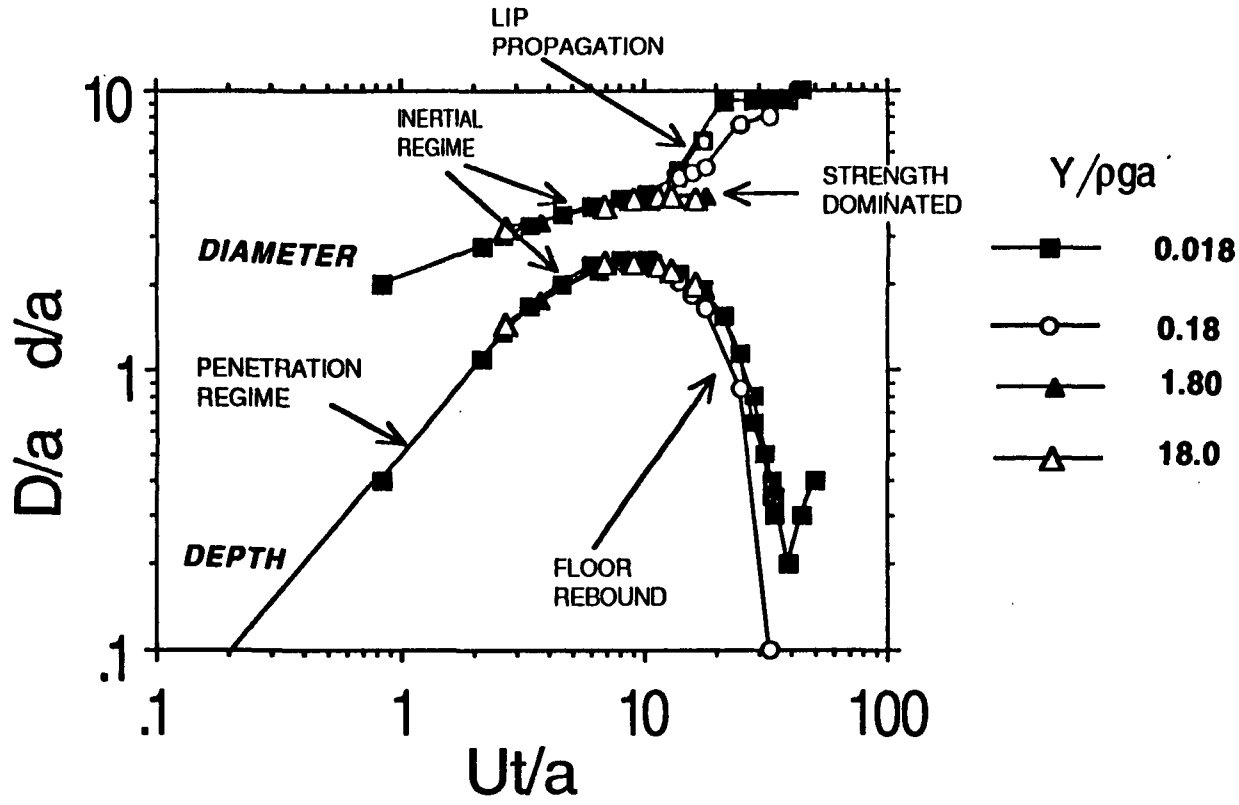

TJA92027SFD

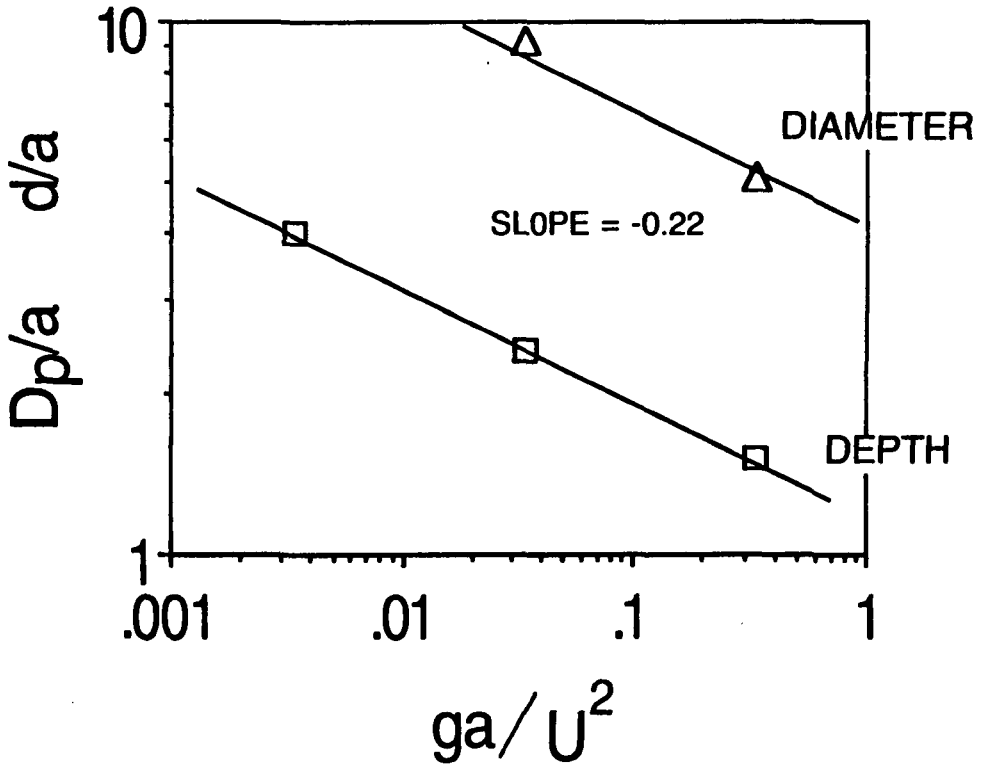

TJA92028SFD

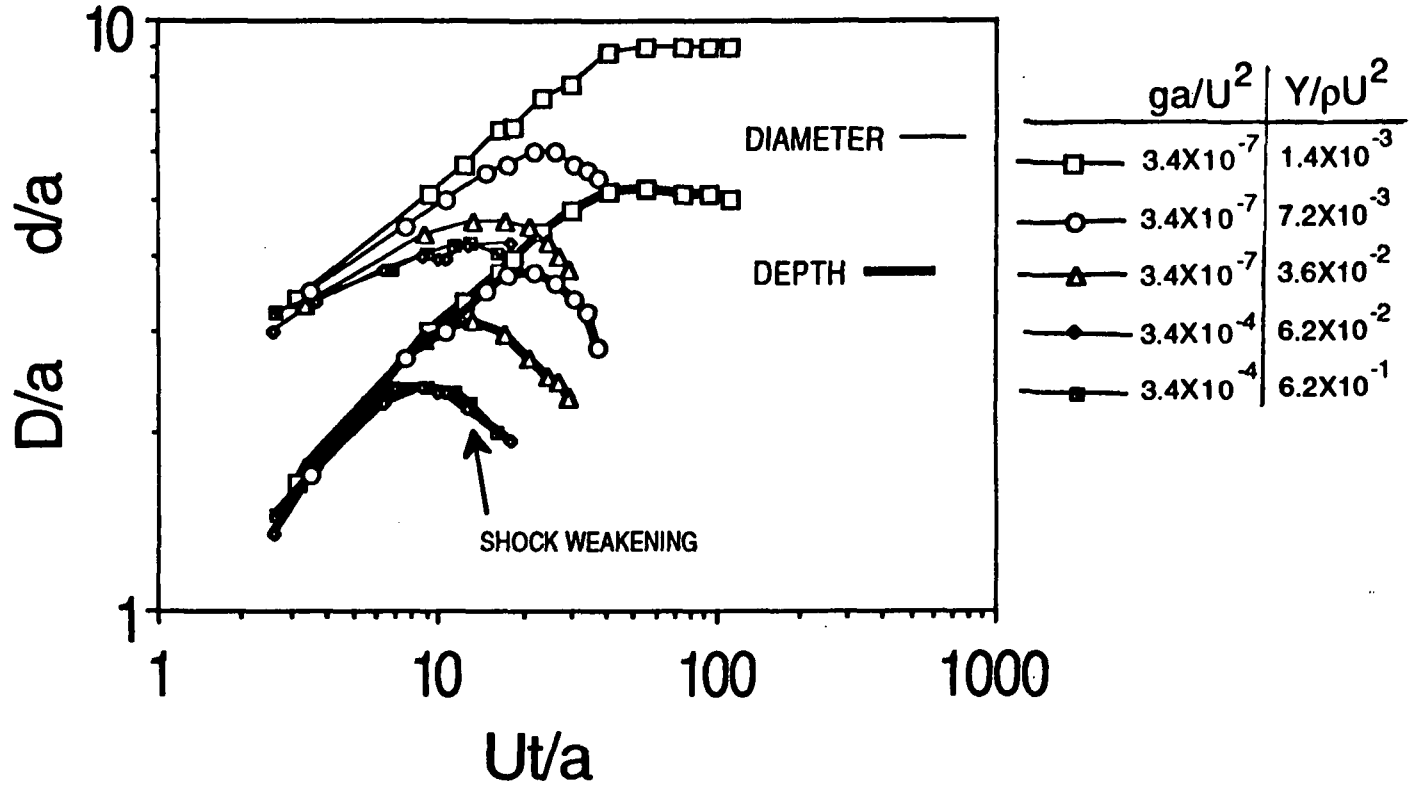
10
1
D/a d/a
1
10
100
1000
Ut/a
DIAMETER
DEPTH
SHOCK WEAKENING
ga/U2 | Y/ρU2
3.4X10-7 | 1.4X10-3
3.4X10-7 | 7.2X10-3
3.4X10-7 | 3.6X10-2
3.4X10-4 | 6.2X10-2
3.4X10-4 | 6.2X10-1

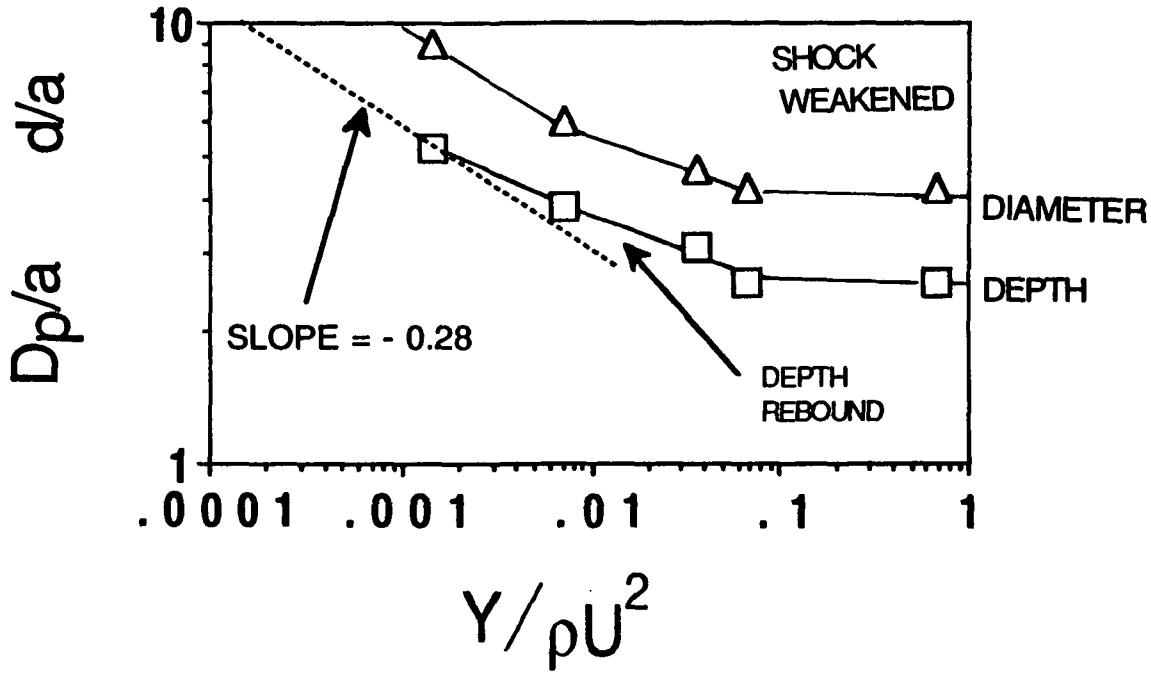
10
1
.0001
.001
.01
.1
1
Dp/a d/a
Y/ρU²
SHOCK
WEAKENED
DIAMETER
DEPTH
SLOPE = - 0.28
DEPTH
REBOUND

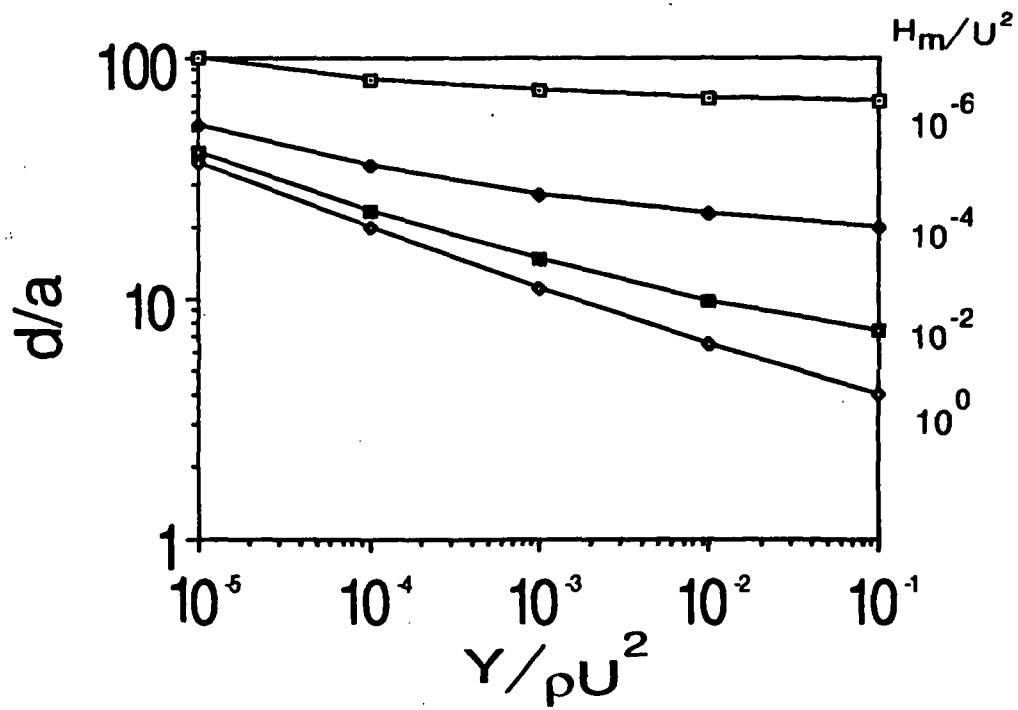
100
10
1
d/a
10^{-5}
10^{-4}
10^{-3}
10^{-2}
10^{-1}
$Y/\rho U^2$
H_m/U^2
10^{-6}
10^{-4}
10^{-2}
10^{0}

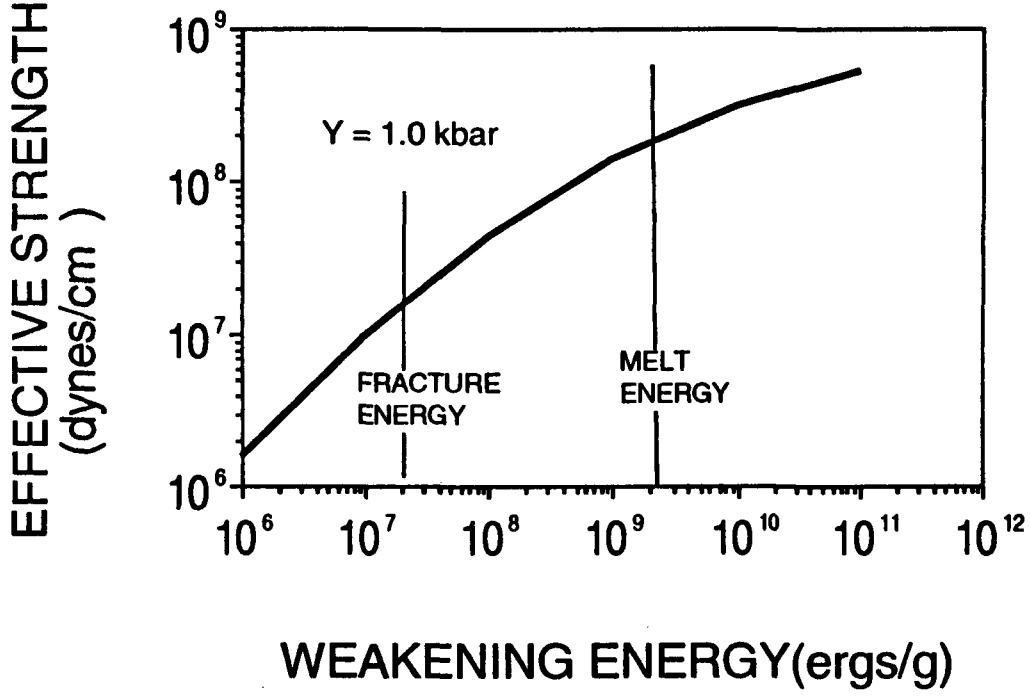
EFFECTIVE STRENGTH
(dynes/cm)
10^9
10^8
10^7
10^6
Y = 1.0 kbar
FRACTURE
ENERGY
MELT
ENERGY
10^6 10^7 10^8 10^9 10^{10} 10^{11} 10^{12}
WEAKENING ENERGY(ergs/g)

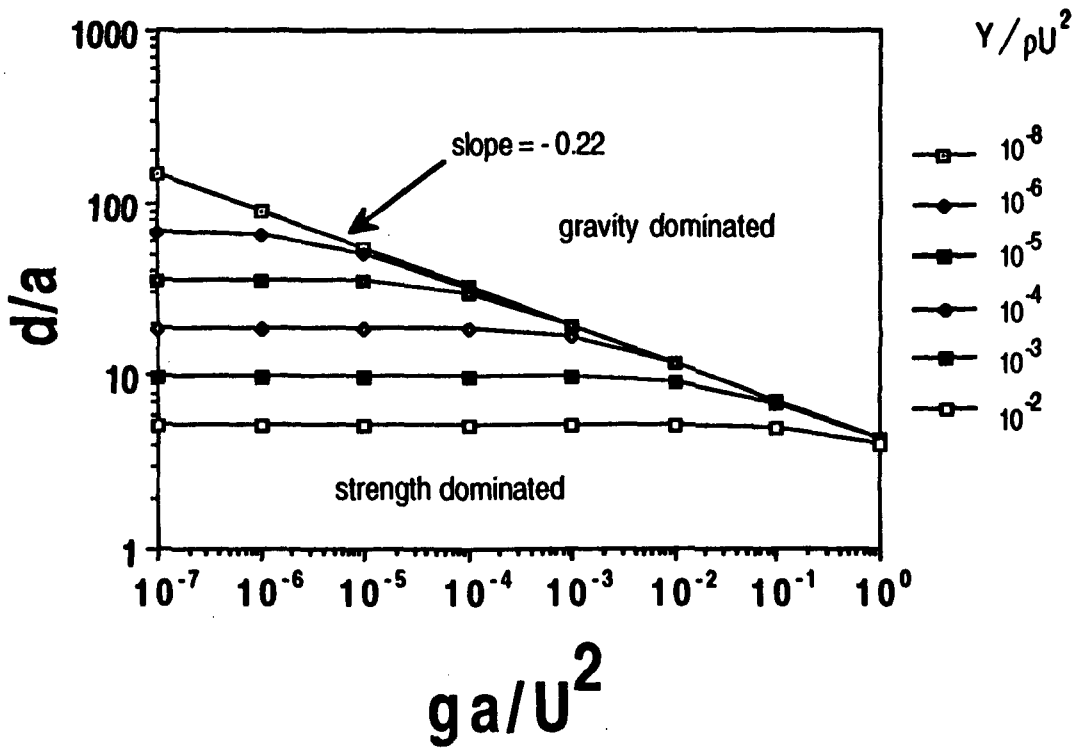
1000
100
10
1
d/a
slope = - 0.22
gravity dominated
strength dominated
10^{-7} 10^{-6} 10^{-5} 10^{-4} 10^{-3} 10^{-2} 10^{-1} 10^{0}
ga/U^2
$Y/\rho U^2$
10^{-8}
10^{-6}
10^{-5}
10^{-4}
10^{-3}
10^{-2}

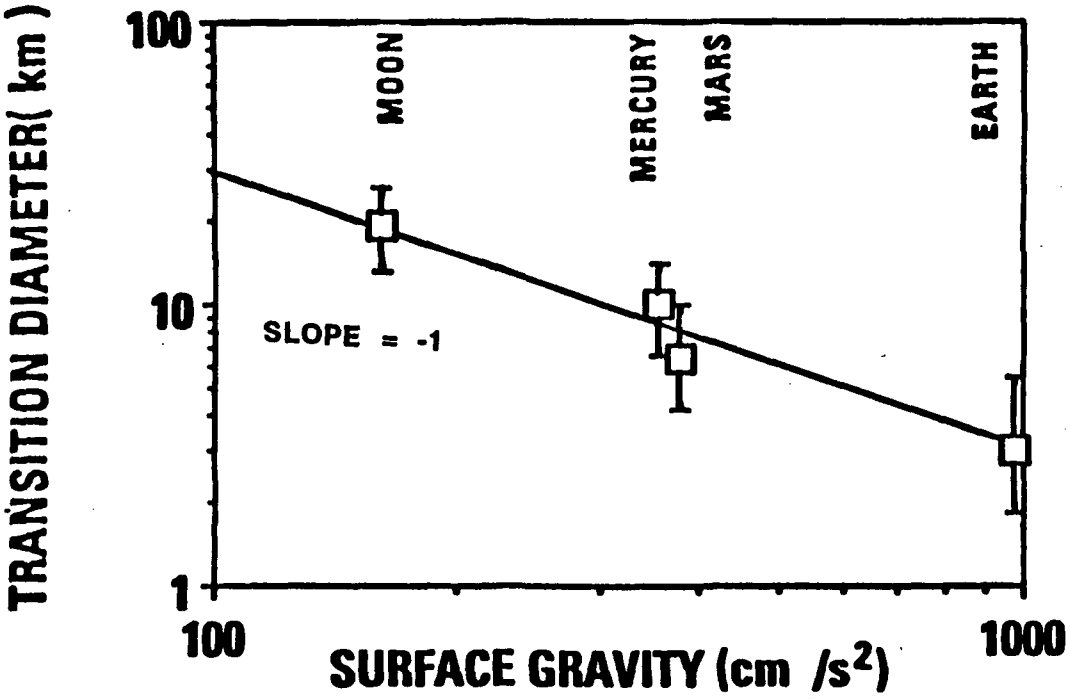
TRANSITION DIAMETER(km)
100
10
1
MOON
MERCURY
MARS
EARTH
SLOPE = -1
100
1000
SURFACE GRAVITY (cm /s²)

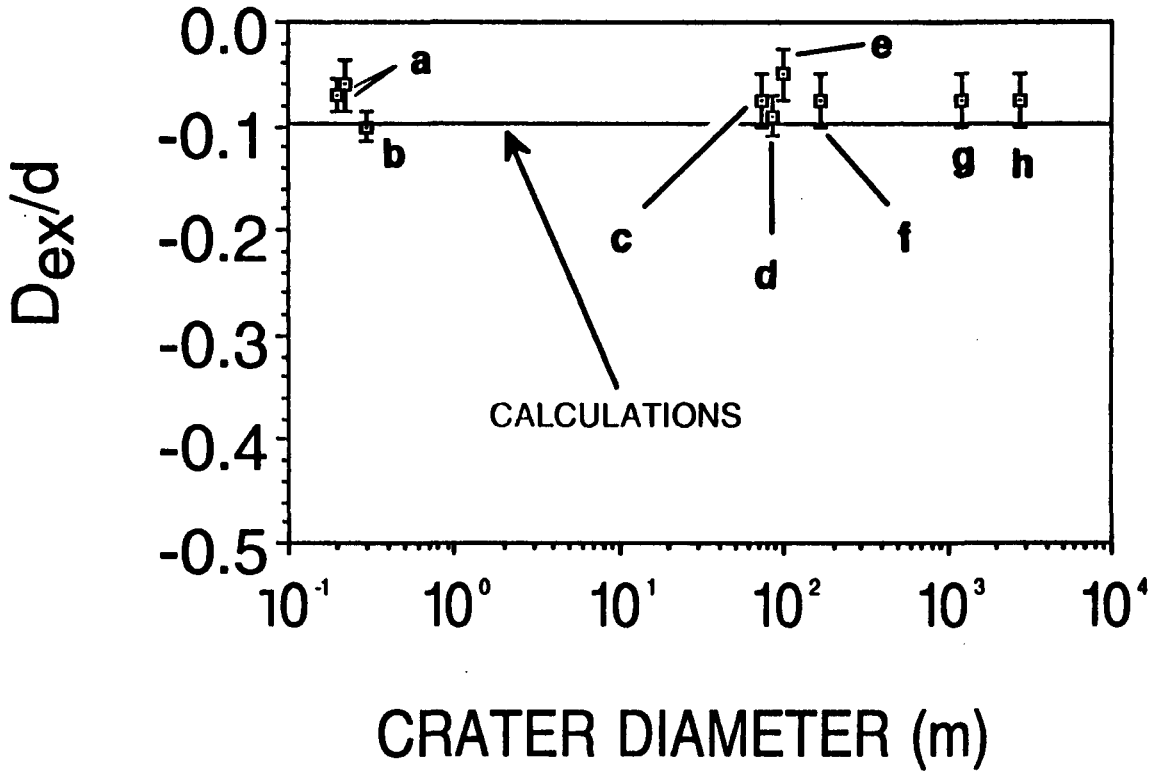

TJA92035SFD

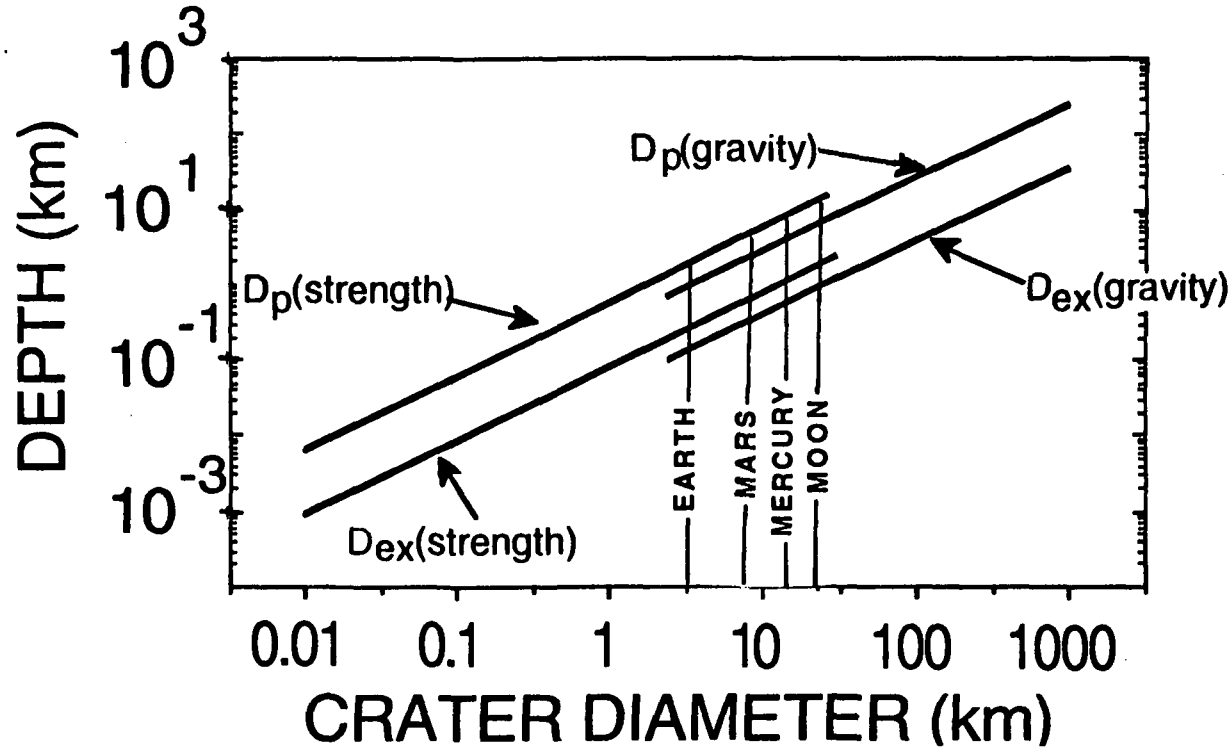
DEPTH (km)
10^3
10^1
10^{-1}
10^{-3}
D_p(gravity)
D_p(strength)
D_{ex}(gravity)
D_{ex}(strength)
EARTH
MARS
MERCURY
MOON
0.01
0.1
1
10
100
1000
CRATER DIAMETER (km)